Petroleum Science 23 (2026) 3616–3633

Contents lists available at ScienceDirect

Petroleum Science

journal homepage: www.keaipublishing.com/en/journals/petroleum-science

Original Paper

Investigation of hydrate inhibitor tracking in oil-gas-water multiphase flow pipelines

Shang-Fei Song [a,*], Jia-Hao Yu [a], Yan-Bo Li [b], Hao-Qi Chen [a], Da-Qian Liu [a], Xiang-Ying Shan [c], Hai-Hong Chen [d], Hai-Yuan Yao [d], Bo-Hui Shi [a,**], Jing Gong [a]

[a] National Engineering Research Center of Oil and Gas Pipeline Transportation Safety/MOE Key Laboratory of Petroleum Engineering/Beijing Key Laboratory of Urban Oil and Gas Distribution Technology, China University of Petroleum (Beijing), Beijing, 102249, China
[b] Beijing Gas Group Co., Ltd., Beijing, 100035, China
[c] Sinopec Engineering Incorporation, Beijing, 100101, China
[d] CNOOC Research Institute Ltd., Beijing, 100028, China

ARTICLE INFO

Article history:
Received 10 April 2025
Received in revised form
9 January 2026
Accepted 11 February 2026
Available online 18 February 2026

Edited by Meng-Jiao Zhou

Keywords:
Hydrate inhibitor tracking
Multiphase pipeline
Multiphase flash calculation
Hydraulic calculation
Thermal calculation

ABSTRACT

As oil and gas exploration progressively moves into deepwater regions, flow assurance in multiphase transport pipelines has become a critical issue. The complex conditions in deepwater environments often lead to the formation of hydrates, which can block pipelines. Therefore, the injection of hydrate inhibitors has become a common practice. In engineering practice, conservative dosing rates are typically adopted to ensure safety margins, but this often leads to a significant increase in costs. This paper presents a steady-state computational model to determine the distribution of inhibitors along the pipeline. The innovation lies in combining multiphase flash calculations with pipeline flow modeling, offering high accuracy and a wide range of applicability. This model is designed with modular flexibility, allowing substitution of different steady-state flow models and thermodynamic models, thereby extending its adaptability to diverse engineering scenarios. The computational results are compared with those from OLGA (a commercial software for multiphase flow simulation), and the results demonstrate that the proposed method achieves high accuracy, indicating that it can serve as a reference for optimizing inhibitor dosage.

1. Introduction

As global energy demand continues to rise, the development of offshore oil and gas resources has become a crucial component of the energy industry (Chen et al., 2025), particularly in the deepwater and ultra-deepwater field exploitation. However, in these harsh environments, the formation of gas hydrates poses a serious threat. Gas hydrates are solid structures composed of natural gas molecules and water under high-pressure (Liu et al., 2023; Li et al., 2025), low-temperature conditions (Meng et al., 2024), resembling ice in appearance (Wei et al., 2024). The environmental conditions in deepwater pipelines are highly conducive to hydrate formation (Xin et al., 2025), which can lead to blockages that disrupt oil and gas transport, increasing operational risks and costs. This phenomenon not only damages equipment but also creates potential safety hazards, posing significant challenges to oil and gas production (Aman, 2021; Sun et al., 2022; Wei et al., 2025; Yu et al., 2025).

To prevent hydrate blockage, the oil and gas industry widely employs thermodynamic hydrate inhibitors (THIs) (Li et al., 2024), such as methanol (MeOH) and monoethylene glycol (MEG), are the most common due to their operational simplicity and proven effectiveness, particularly in long-distance pipelines and deepwater fields (Brustad et al., 2005; Nasir et al., 2020; Alavi and Sharifzadeh, 2024; Kashish et al., 2024). THIs suppress hydrate formation by shifting the thermodynamic equilibrium conditions. However, large-scale use involves significant chemical consumption, high storage and transportation costs, and potential environmental risks. Typical MeOH or MEG injection rates range from

* Corresponding author.
** Corresponding author.
E-mail addresses: song.sf@cup.edu.cn (S.-F. Song), bh.shi@cup.edu.cn (B.-H. Shi).
Peer review under the responsibility of China University of Petroleum (Beijing).

https://doi.org/10.1016/j.petsci.2026.02.015

20% to 50% of the aqueous phase mass, with additional safety margins often applied to ensure flow assurance (Huang, 2011; Sahari Moghaddam et al., 2022; Bakhtyari et al., 2024; Costa do Nascimento et al., 2025). Moreover, the effectiveness of THIs is highly sensitive to flow conditions, terrain variations, and the distribution of water content along the pipeline, often leading to uneven inhibitor dispersion and localized failure. Although low-dosage hydrate inhibitors (LDHIs) have been applied in certain scenarios (Javanmardi et al., 2024), such as green and low-dosage kinetic hydrate inhibitors derived from biomass or agricultural waste (Oyefunke Olarinoye et al., 2024), THIs remain the mainstream solution in complex deepwater systems. A key challenge is therefore to optimize THIs injection volumes and spatial distribution, ensuring effective hydrate prevention while minimizing chemical overuse and associated costs.

Research on inhibitor tracking algorithms remains limited. However, since inhibitors are simply one component of the flowing mixture, their transport can be modeled using compositional tracking approaches. Prior work on compositional tracking has focused mainly on natural gas pipeline simulation and typically adopts transient formulations. Guandalini et al. (2017)simplified the momentum equation and solved a single pipeline transient hydraulics problem, proposing an energy-based (rather than volumetric) formulation for pipeline flow analysis. Chaczykowski and Zarodkiewicz (2017) employed a similar strategy to track the calorific value parameter under transient conditions and accounted for temperature variations by solving the energy equation. Chaczykowski et al. (2018) further introduced the compositional transport equation to analyze species migration in a single pipe. Fan et al. (2021) proposed a finite volume, network-scale compositional tracking method using a discrete solution approach with a first-order upwind scheme, which performs well when compositions remain stable. Bermúdez and Shabani (2022) combined second-order finite element thermohydraulic simulation with a first-order explicit method of characteristics for composition tracking, significantly improving computational efficiency, albeit with limitations in adaptivity and time-step selection.

In addition, current compositional tracking methods can accurately calculate changes in components along their path, but most research has focused on natural gas components. As a special component, inhibitors are distributed across all three phases—gas, oil, and water. Under steady-state conditions, employing three-phase flash calculations enables the precise determination of inhibitor distribution. In current commercial software (such as OLGA), although the built-in phase equilibrium software Multiflash is incorporated, the inhibitor tracking module does not include rigorous three-phase flash calculations.

The steady-state tracking of inhibitors primarily involves calculating fluid flow characteristics within the pipeline and the corresponding inhibitor distribution. Research on the flow characteristics of gas-liquid two-phase pipelines is relatively mature (Ovadia, 2006), so in inhibitor tracking simulations in this research, the focus is on predicting the inhibitor distribution after injection. This paper employs multiphase flash calculations as the method for predicting inhibitor distribution. This approach, grounded in thermodynamic principles, accurately accounts for the distribution of substances across phases, offering higher precision and broader applicability. Unlike empirical methods and data models, multiphase flash calculations exhibit stable and reliable characteristics while requiring a reduced volume of data.

Epelle et al. (2021) compared various equations of state (EoS) for inhibitor distribution in hydrate systems, identifying the most accurate method. They (Epelle et al., 2020) used the Huron-Vidal rule and SRK equation for MEG and MeOH concentrations, with errors under 5%. Folas et al. (2007) used the CPA equation for MEG, achieving high accuracy. These studies confirm the effectiveness of multiphase flash calculations. These studies confirm the effectiveness of multiphase flash calculations.

Therefore, based on a multiphase flash calculation model, this study proposes a flexible and comprehensive steady-state simulation model that integrates multiphase flow hydraulics, thermal calculations, and thermodynamic phase equilibrium analysis. A new method is developed to predict the spatial distribution of hydrate inhibitors (e.g., MeOH and MEG) in long-distance multiphase pipelines. While current research offers various solutions for inhibitor tracking, many existing approaches rely on fixed internal model couplings, empirical assumptions, or require fully transient simulations. In contrast, the method presented in this work features a modular architecture, allowing the substitution of any steady-state pressure drop model, temperature model, or EoS. Moreover, multiphase flash calculations are performed under steady-state conditions to enable physically consistent and accurate prediction of inhibitor distribution across phases. Compared to existing empirical or data-driven methods, this model improves the reliability of inhibitor distribution prediction, enhances adaptability to diverse flow conditions, and maintains computational efficiency suitable for engineering design and analysis. It should be noted that, compared to the static sub-function substitution employed in traditional methods, our model framework offers a more flexible structure through modular design, enabling dynamic adjustment of individual components according to specific circumstances. Whereas conventional approaches are often constrained by predetermined computational structures, our model flexibly integrates diverse pipeline flow models and flash calculation models. This enables it to deliver more precise and applicable solutions across varying topographies, environmental conditions, and operational modes. Such adaptability not only enhances the model's versatility but also amplifies its potential for application in complex scenarios.

2. Calculation model for hydrothermal and phase equilibrium

The steady-state inhibitor tracking model developed in this study comprises two main parts, the first involves the establishment of a coupled hydrothermal model, including the hydraulic model, the thermal model, and their integration. The second focuses on the development of the multiphase steady-state pipeline inhibitor tracking model, encompassing the establishment of the multiphase pipe-section model, the simulation algorithm, and the flash calculation module.

2.1. Model assumptions

To ensure the model's validity and applicability, we have made certain assumptions within the model. These assumptions simplify the complexity of the actual system and render the computational process more efficient.

1) The pipeline is operating under steady-state flow conditions.
2) All heat transfer phenomena in the pipeline are set as a total heat transfer coefficient.
3) The pipeline is divided into several small pipe sections during calculation. The inlet and outlet pressure and temperature of each small section are calculated using steady-state hydraulic and thermal models, with the outlet conditions of the upstream section serving as the inlet conditions for the downstream section. This approach is referred to as a marching algorithm (Brill and Mukherjee, 1999). For output purposes, the average

pressure and temperature of each section are taken as its output results.
4) Within each pipe section, a flash calculation is performed using average temperature and pressure to determine the fluid phase distribution and thermophysical properties.
5) When performing hydraulic calculations on pipelines, it is assumed that the liquid phase within the pipeline consists of a stable oil-water emulsion. For flash calculations, a three-phase gas-oil-water flash model is employed.
6) The local mechanical energy loss caused by changes in pipeline inclination can be considered negligible compared to the friction loss along the pipeline.

2.2. Hydrothermal model

2.2.1. Hydraulic calculation model

In the calculation of pressure distribution in multiphase flow pipes, various models have been proposed to deal with complex flow conditions (Li et al., 2026). Common models include the Drift-Flux model (Wallis, 2020), the Lockhart-Martinelli model (Lockhart, 1949), the Taitel-Dukler model (Taitel and Dukler, 1976), and the Beggs-Brill model (Beggs and Brill, 1973), each of which has its own applicable scenarios and limitations. The Drift-Flux model describes gas-liquid phase slip velocity well, especially for stratified flows in large pipes, but its accuracy decreases for complex patterns like annular flows. The Lockhart-Martinelli model, effective for horizontal two-phase flow pressure prediction, struggles with inclined pipes and complex flow patterns due to limited flow pattern consideration. The Taitel-Dukler model predicts gas-liquid flow transitions well but is hindered by complex flow determination and high computational costs. In contrast, the Beggs-Brill model offers flexible empirical correlations, handling multiphase flows in inclined and horizontal pipes effectively, with accurate pressure distribution predictions under steady-state conditions through liquid volume fraction and frictional pressure estimation.

However, the Beggs-Brill model, though widely used, has limited accuracy in steep inclinations and complex flow regimes, such as slug or annular flow, due to its reliance on discrete flow pattern maps and empirical correlations.

To overcome these limitations, several improved models have been developed. The Mukherjee-Brill model (Mukherjee and Brill, 1985) extends the Beggs-Brill model using a larger experimental dataset and refined correlations, enhancing prediction accuracy in inclined and vertical pipes. The Unified mechanistic model (Zhang et al., 2003), grounded in conservation equations and continuous formulations, avoids explicit flow regime switching and ensures better physical consistency in complex terrain or flow transitions.

In this study, the Beggs-Brill model is chosen as the baseline due to its simplicity, computational stability, and broad industrial adoption under steady-state conditions. Notably, the proposed inhibitor tracking model is modular and supports substitution of different steady-state flow models, enabling flexible adaptation to various pipeline geometries and terrain complexities. To illustrate this flexibility, sensitivity analyses employing the Mukherjee-Brill and Unified models are conducted and discussed in Section 3.3.

(1) Derivation of pressure distribution equation (Beggs and Brill, 1973)

For fluid flow calculations, an energy balance equation can be applied. Assuming steady-state conditions and no external work on or by the fluid, the differential form of the mechanical energy balance equation is given by:

$$\frac{\mathrm{d}P}{\rho}+g\mathrm{d}H+u\mathrm{d}u+\mathrm{d}\left(W_{\mathrm{f}}\right)=0 \tag{1}$$

where P is pressure, in Pa; ρ is fluid density, in kg/m^3; g is gravitational acceleration, in m/s^2; H is elevation, in m; u is velocity, in m/s; d(W_{f}) represents the irreversible frictional losses, in m^2/s^2. For flow along an inclined pipe, the vertical distance moved is:

$$\mathrm{d}H=\sin\theta\,\mathrm{d}L \tag{2}$$

where θ is the angle of the pipe from the horizontal, in degrees; L is the axial distance along the pipe, in m. Substituting this into the energy balance equation, we obtain:

$$\frac{\mathrm{d}P}{\mathrm{d}L}=-\left[g\rho\sin\theta+\rho u\frac{\mathrm{d}u}{\mathrm{d}L}+\rho\frac{\mathrm{d}\left(W_{\mathrm{f}}\right)}{\mathrm{d}L}\right] \tag{3}$$

Thus, the pressure gradient can be viewed as consisting of three components:

$$-\frac{\mathrm{d}P}{\mathrm{d}L}=F_{\mathrm{el}}+F_{\mathrm{acc}}+F_{\mathrm{f}} \tag{4}$$

This indicates that the total pressure gradient is the sum of the pressure losses due to changes in potential energy, kinetic energy, and friction.

For the friction pressure distribution:

$$F_{\mathrm{f}}=\frac{f\rho u^2}{2d} \tag{5}$$

where f is the friction factor, and d is the pipe diameter, in m.

The acceleration term, representing changes in kinetic energy, is often negligible for most practical cases. The mixture velocity can be expressed as the sum of the liquid and gas phase velocities:

$$u=\frac{G_{\mathrm{L}}}{\rho_{\mathrm{L}}}+\frac{G_{\mathrm{g}}}{\rho_{\mathrm{g}}} \tag{6}$$

where G_{L} and G_{g} are the mass flux rates of the liquid and gas phases, in kg/(s·m^2); ρ_{L} and ρ_{g} are their respective densities, in kg/m^3. The acceleration pressure gradient is then given by:

$$F_{\mathrm{acc}}=\rho u\frac{\mathrm{d}u}{\mathrm{d}L}=\rho u\left[\frac{\mathrm{d}}{\mathrm{d}L}\left(\frac{G_{\mathrm{L}}}{\rho_{\mathrm{L}}}\right)+\frac{\mathrm{d}}{\mathrm{d}L}\left(\frac{G_{\mathrm{g}}}{\rho_{\mathrm{g}}}\right)\right] \tag{7}$$

Since gas is much more compressible than liquid, it can be approximated that:

$$\frac{\mathrm{d}}{\mathrm{d}L}\left(\frac{G_{\mathrm{L}}}{\rho_{\mathrm{L}}}\right)\approx 0 \tag{8}$$

Thus, the acceleration pressure gradient is primarily influenced by the gas phase:

$$F_{\mathrm{acc}}\approx\rho u\frac{\mathrm{d}}{\mathrm{d}L}\left(\frac{G_{\mathrm{g}}}{\rho_{\mathrm{g}}}\right)=\rho u\left[\frac{\frac{\mathrm{d}}{\mathrm{d}L}\left(G_{\mathrm{g}}\right)}{\rho_{\mathrm{g}}}-\frac{G_{\mathrm{g}}}{\rho_{\mathrm{g}}^2}\frac{\mathrm{d}}{\mathrm{d}L}\left(\rho_{\mathrm{g}}\right)\right] \tag{9}$$

It can be assumed that the change in gas mass flux is much smaller than the change in gas density:

$$\frac{\mathrm{d}}{\mathrm{d}L}\left(G_{\mathrm{g}}\right)\ll\frac{G_{\mathrm{g}}}{\rho_{\mathrm{g}}^2}\frac{\mathrm{d}}{\mathrm{d}L}\left(\rho_{\mathrm{g}}\right) \tag{10}$$

The rate of change in gas density is then approximated using the real gas law as:

$$\frac{\mathrm{d}}{\mathrm{d}L}(\rho_g) = \frac{\mathrm{d}}{\mathrm{d}L}\left(\frac{pM_w}{z_g RT}\right) = \frac{M}{z_g RT}\frac{\mathrm{d}p}{\mathrm{d}L} + \frac{p}{z_g RT}\frac{\mathrm{d}M_w}{\mathrm{d}L} - \frac{M_w p}{z_g^2 RT}\frac{\mathrm{d}z_g}{\mathrm{d}L} - \frac{M_w p}{z_g RT^2}\frac{\mathrm{d}T}{\mathrm{d}L} = \rho_g\left(\frac{1}{p}\frac{\mathrm{d}p}{\mathrm{d}L} + \frac{1}{M_w}\frac{\mathrm{d}M_w}{\mathrm{d}L} - \frac{1}{z_g}\frac{\mathrm{d}z_g}{\mathrm{d}L} - \frac{1}{T}\frac{\mathrm{d}T}{\mathrm{d}L}\right) \tag{11}$$

where z_g is gas compressibility factor; M_w is molecular weight, in g/mol; T is temperature, in K.

Neglecting the smaller terms:

$$\frac{1}{M_w}\frac{\mathrm{d}M_w}{\mathrm{d}L} - \frac{1}{z_g}\frac{\mathrm{d}z_g}{\mathrm{d}L} - \frac{1}{T}\frac{\mathrm{d}T}{\mathrm{d}L} \ll \frac{1}{p}\frac{\mathrm{d}p}{\mathrm{d}L} \tag{12}$$

We arrive at the simplified form of the acceleration pressure gradient:

$$F_{acc} = -\rho u\frac{G_g}{\rho_g^2}\frac{\mathrm{d}}{\mathrm{d}L}(\rho_g) = -\rho u\frac{G_g}{\rho_g^2}\frac{\rho_g}{p}\frac{\mathrm{d}p}{\mathrm{d}L} = -\frac{\rho u u_{sg}}{p}\frac{\mathrm{d}p}{\mathrm{d}L} \tag{13}$$

The pressure gradient due to elevation change is given by:

$$F_{el} = g\rho\sin\theta \tag{14}$$

To account for both phases, the mixture density is calculated using the liquid holdup H_L (Beggs and Brill, 1973):

$$\rho = \rho_L H_L + \rho_g(1 - H_L) \tag{15}$$

Thus, the elevation pressure gradient can be written as:

$$F_{el} = g[\rho_L H_L + \rho_g(1 - H_L)]\sin\theta \tag{16}$$

By combining the frictional, acceleration, and elevation terms, the total pressure gradient equation is:

$$-\frac{\mathrm{d}P}{\mathrm{d}L} = g\rho\sin\theta + \frac{fGu}{2d} - \frac{\rho u u_{sg}}{p}\frac{\mathrm{d}P}{\mathrm{d}L} \tag{17}$$

where u_{sg} represents superficial gas velocity, in m/s.

Based on the aforementioned derivation process, the final form of the pressure gradient equation can be expressed as:

$$-\frac{\mathrm{d}P}{\mathrm{d}L} = \frac{g[\rho_L H_L + \rho_g(1 - H_L)]\sin\theta + \frac{fGu}{2d}}{\left(1 - \frac{[\rho_L H_L + \rho_g(1-H_L)]u u_{sg}}{p}\right)} \tag{18}$$

The flow pattern classification and inclination correction factors are not elaborated here, and can be referred to in the original Beggs-Brill model (Beggs and Brill, 1973) reference.

(2) Closure relation

In Beggs-Brill model, the friction factor f is given by:

$$\frac{f}{f_{ns}} = \mathrm{e}^S \tag{19}$$

where e is natural constant; f_{ns} is the no-slip friction factor S is given by:

$$S = \frac{\ln y}{-0.0523 + 3.18\ln y - 0.8725(\ln y)^2 + 0.01853(\ln y)^4}$$
$$y = \frac{\lambda}{H_L^2} \tag{20}$$

$$\lambda = \frac{q_L}{q_L + q_g} \tag{21}$$

where λ is input liquid content. q is in-situ volumetric flow rate, in m^3/s. When $1 < y < 1.2$, $S = \ln(2.2y - 1.2)$.

The no-slip friction factor f_{ns} is given by:

$$f_{ns} = \left[2\lg\left(\frac{N_{Rens}}{4.5223\lg N_{Rens} - 3.8215}\right)\right]^{-2} \tag{22}$$

where

$$N_{Rens} = \frac{[\rho_L\lambda + \rho_g(1-\lambda)]ud}{\mu_L\lambda + \mu_g(1-\lambda)} \tag{23}$$

where μ_L is liquid viscosity and μ_g is gas viscosity, in Pa·s; N_{Rens} is the Reynolds number.

In hydraulic calculations, the liquid phase represents an oil-water mixture. Therefore, when using hydraulic models for computation, the parameters of the oil phase and water phase must be combined into a single phase. The mixing rules employed in this paper are as follows.

For density, the commonly used volume fraction mixing rule is applied.

$$\rho_L = \rho_o V_{f,o} + \rho_w V_{f,w} \tag{24}$$

where, ρ_o and ρ_w denote the densities of the oil phase and water phase, respectively, and V_f represents the volume fraction, and the detailed formula is provided in the Supplementary data. ρ_L is the density of the liquid phase after mixing.

For viscosity, the Katti-Chaudhri (Katti and Chaudhri, 1964) mixing rule is employed.

$$\ln(\mu_L V_L) = x_o\ln(\mu_o V_o) + x_w\ln(\mu_w V_w) \tag{25}$$

$$V_L = x_o V_o + x_w V_w \tag{26}$$

where, x_o and x_w denote the molar fractions of the oil phase and water phase, respectively. V_o and V_w denote the molar volumes of the oil phase and water phase, respectively. μ_o and μ_w denote the viscosities of the oil phase and water phase, respectively. μ_L denotes the viscosity of the mixed liquid phase. V_L denotes the volume of the mixed liquid phase.

2.2.2. Thermal model

The temperature distribution calculation employs the widely recognized multiphase flow pipeline temperature distribution formula (Yu et al., 2000), taking into account the Joule-Thomson effect:

$$T_e = (T_a + B) + (T_s - T_a - B)\mathrm{e}^{-AL} - D_i\frac{X_{wg}c_{pg}}{c_p}\left(\frac{P_s - P_e}{AL}\right)\left(1 - \mathrm{e}^{-AL}\right) \tag{27}$$

$$A = \frac{k\pi D}{Mc_p},\ B = \frac{ig(1 - x_{wg})}{Ac_p} \tag{28}$$

in the equation, T_s and T_e represent the temperatures at the starting and ending points of the pipeline section, respectively, in K; P_s and P_e are the pressures at the starting and ending points of the pipeline section, respectively, in Pa; T_a is the ambient temperature, in K; L is the axial distance along the pipe, in m; X_{wg} is the gas-phase mass

fraction; k is the overall heat transfer coefficient, in W/(m^2·K); D_i is the Joule-Thomson coefficient, in K/Pa, and the detailed formulas are provided in the Supplementary data; C_{pg} is the specific heat capacity of the gas at constant pressure, in J/(kg·K); C_p is the specific heat capacity of the mixture at constant pressure, also in J/(kg·K); M is the mass flow rate of the gas-liquid mixture, in kg/s; and i is the hydraulic gradient of the liquid, in m/m.

$$i = \frac{P_s - P_e}{g \times \rho_L \times L} \tag{29}$$

Due to the fluctuations in terrain that can lead to changes in liquid holdup, to ensure that the calculation results align with reality, the effect of liquid holdup variation on temperature distribution is taken into account. The specific heat calculation formula is as follows (Yu et al., 2000):

$$c_p = [\,1 - H_L(\theta)\,] \times c_{pg} + H_L(\theta) \times c_{pL} \tag{30}$$

in the equation, $H_L(\theta)$ represents the liquid holdup at an inclination angle of θ, in degrees; C_{pL} is the specific heat capacity of the liquid at constant pressure, measured in J/(kg·K).

2.2.3. Coupled hydrothermal modeling

As evident from the temperature distribution calculation formula, the inlet and outlet pressures of the pipeline section are known parameters. When the pipeline section temperature changes, the calculated properties of the gas and liquid phases also change, which in turn affects the calculation of the pressure distribution across the section. Therefore, temperature indirectly influences the pressure distribution calculation (Zhang, 2014), necessitating a coupled temperature and pressure calculation.

The computational flow of the hydraulic and thermal coupling model is shown in Fig. 1.

As shown in Fig. 1, the calculation steps for hydrothermal coupling are as follows:

1) For each pipeline section, initial estimates of pressure drop ΔP and temperature drop ΔT are assumed. These are used to compute the outlet pressure P_e and outlet temperature T_e, followed by the section's average pressure P_{avg} and temperature T_{avg}.
2) A three-phase flash calculation is performed at P_{avg} and T_{avg} to obtain fluid thermophysical properties. These are used to determine the flow regime, liquid holdup, inclination correction factor, and the friction factor.
3) Using the obtained parameters, the pressure and temperature drop equations are applied to calculate updated values ΔP and ΔT.
4) The calculated values are compared with the initial estimates. If the differences are within specified tolerances, the iteration

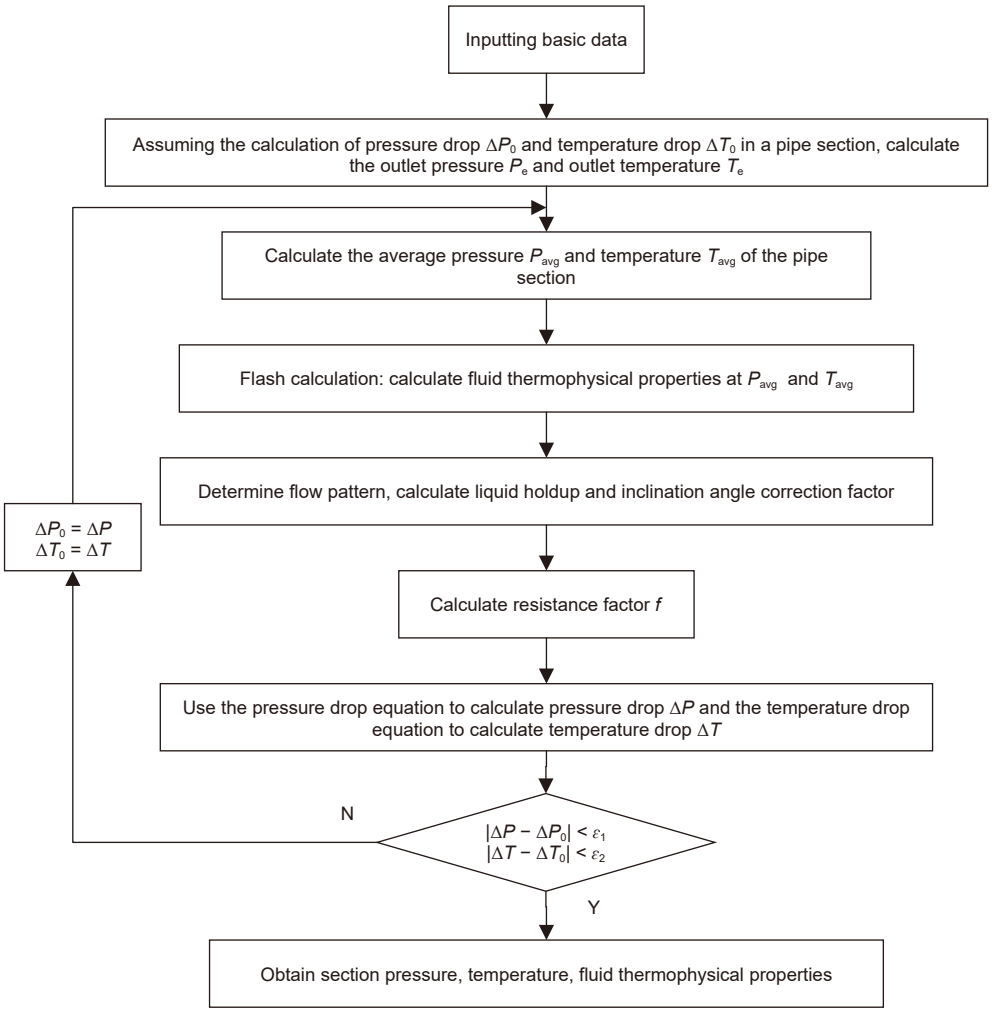

Fig. 1. Flow chart of hydraulic and thermal coupling calculation of pipe section.

converges and the section's results are stored; otherwise, the estimates are updated and the procedure repeats.

A detailed description of the flash method can be found in Section 2.2.2.

2.3. Multiphase pipeline inhibitor tracking simulation

2.3.1. Multiphase flow pipeline modeling

Fig. 2 illustrates the schematic diagram of the control volume model used in this paper. The fluid within a ΔL pipeline section is taken as the control volume, where the fluid flows in from upstream, subsequently moving towards the downstream of the control volume. The fluid within the pipeline comprises a three-phase mixture of oil, gas, and water.

In the model, the pipeline is first discretized into grids, with the upstream node of the control volume indexed as $n-1$, the downstream node indexed as n. x represents the mole fraction of any component and Q represents the flow rate.

The overall calculation process is as follows:

(1) Input the basic data, encompassing: fluid pressure, temperature, composition, and mass flow rate at the pipeline inlet; pipeline diameter, wall thickness; mileage and elevation along the pipeline route; ambient temperature; overall heat transfer coefficient; and other relevant parameters. Determine the number of pipeline sections N_o, section length ΔL, initial pressure P_s at the starting point of the inlet section, and temperature T_s, serving as pipeline inlet conditions.

(2) Initially, assume the pressure drop ΔP_0 and temperature drop ΔT_0 for the first zone to derive P_e, T_e, P_{avg} and T_{avg} of the whole zone. Based on these average values, determine parameters such as mole fraction, mass fraction, density, viscosity, and surface tension for the oil, gas, and water phases using the flash calculation model.

(3) Next calculate the zones after the first pipe section, using the pressure and temperature at the outlet of the previous pipe section as the inlet pressure and temperature of the calculated section, with the remaining calculations being the same as in step (2).

(4) Using the parameters obtained from step (2), the pressure drop ΔP and temperature drop ΔT are calculated by the thermohydraulic model. Then, it is determined whether the conditions $|\Delta P - \Delta P_0| < \varepsilon_1$ and $|\Delta T - \Delta T_0| < \varepsilon_2$ hold true. If they do, proceed to the next step; if not, set $\Delta P_0 = \Delta P$ and $\Delta T_0 = \Delta T$, and return to step (3).

(5) After calculating the temperature and pressure of the pipeline, determine the fluid composition within each pipe section, and then the distribution of the inhibitor components in the three phases is obtained from the results of the flash calculations.

(6) If $n > N_o$ holds true, proceed to the next step; otherwise, set $n = n + 1$, use the endpoint conditions of the previous pipeline section as the starting conditions for the next section, and return to step (2). Loop the calculation to the last pipe section, end the calculation and output the result.

The overall simulation flow is shown in Fig. 3.

2.3.2. Inhibitor tracking simulation

In the study of phase behavior of petroleum fluids, multiphase flash calculations are usually performed using cubic type EoS (Lei et al., 2025). In this paper, the gas-liquid phase distribution prediction of natural gas condensate is carried out using the well-adapted PR (Peng-Robinson) EoS (Peng and Robinson, 1976), which can be expressed as:

$$p = \frac{RT}{V-b} - \frac{a}{V(V+b)+b(V-b)} \tag{31}$$

where a and b are two characteristic parameters. For a pure substance consisting of a single component, a and b can be found directly in the reference (Tianmin, 2002); for a mixture consisting of multiple components, a and b are derived from the parameters of the individual components that make up the fluid according to a specific mixing rule. For mixtures, HuronVidal mixing rule is adopted. The HuronVidal mixing rule introduces excess Gibbs energy from activity coefficient models into the EoS, significantly improving the accuracy of liquid-phase non-ideality predictions, especially for highly non-ideal and polar systems (Huron and Vidal, 1979).

For a given composition, temperature, and pressure, multiphase flash calculation must satisfy the following conditions.

The fugacity of each component must be equal in all coexisting phases (Chen et al., 2024):

$$F_i^1 = F_i^2 = \cdots = F_i^{N_p},\ i = 1, \cdots, N_C \tag{32}$$

where F is fugacity, in Pa.

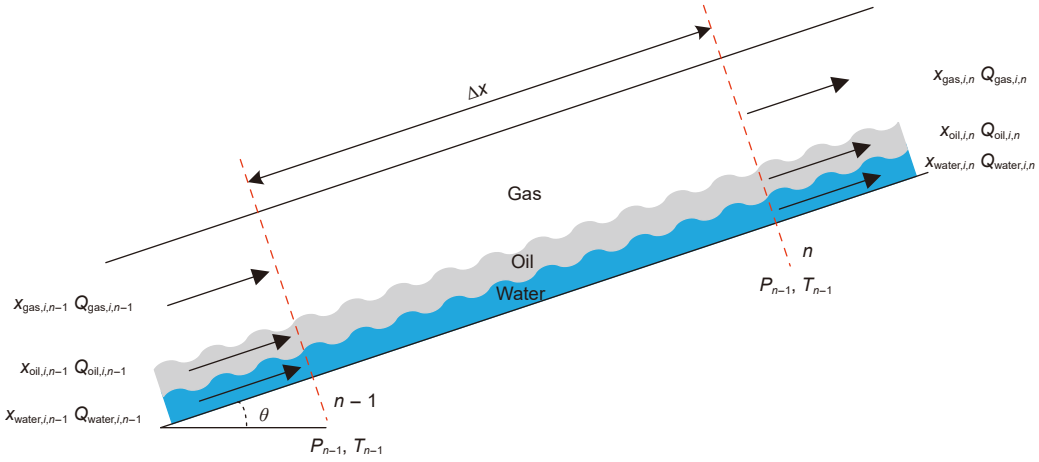

Fig. 2. Schematic diagram of pipe section model.

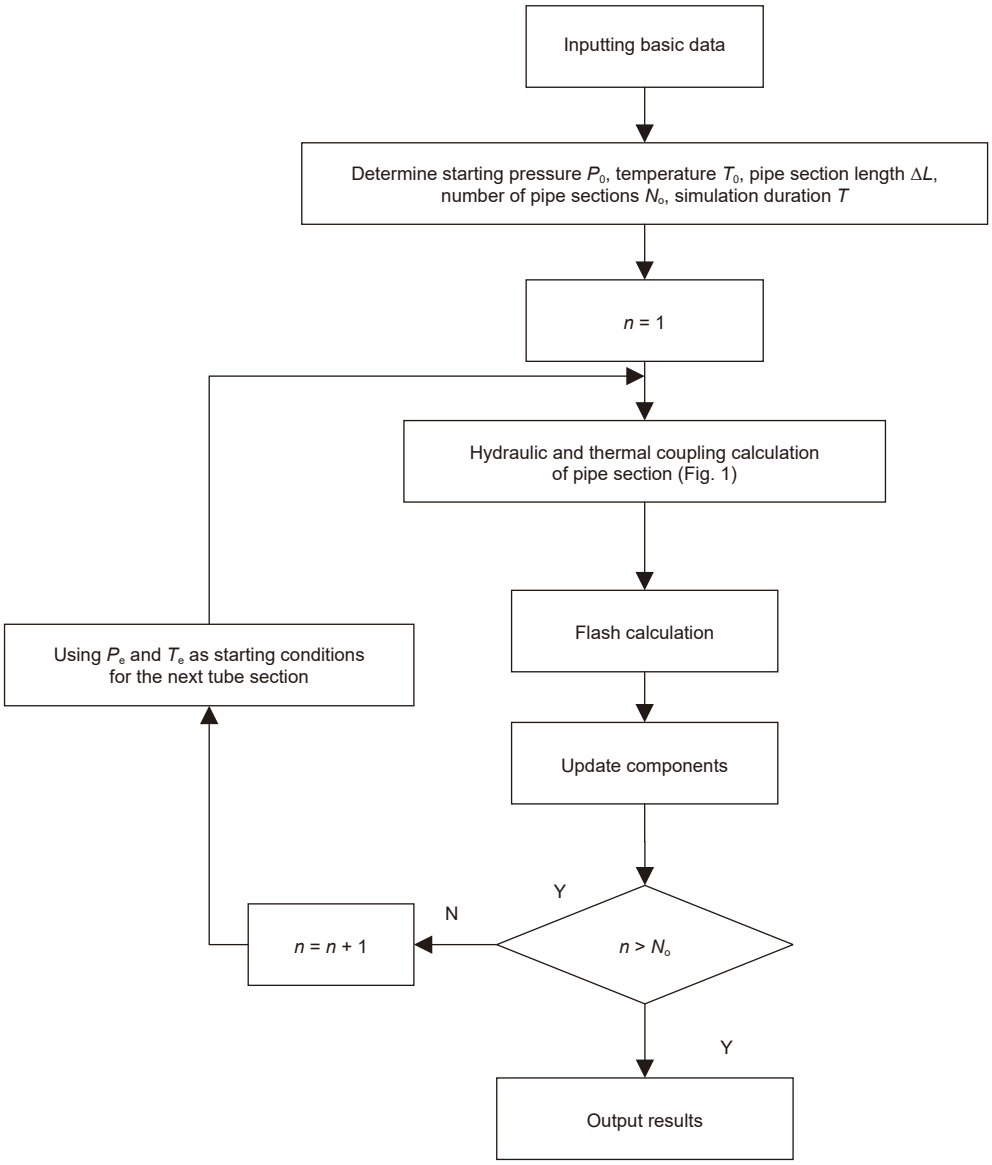

Fig. 3. Steady-state inhibitor tracking calculation flow chart.

The phase fractions within the system must satisfy overall phase fraction conservation:

$$\sum_{j=1}^{N_P} \alpha^j = 1 \tag{33}$$

Component-wise material balance must be satisfied across all phases:

$$\sum_{j=1}^{N_P} c_i^j \alpha^j = z_i,\ i = 1, \cdots, N_C \tag{34}$$

$$\sum_{i=1}^{N_P} c_i^j = 1,\ j = 1, \cdots, N_P \tag{35}$$

The phase with the highest density is selected as the reference phase (denoted as N_P*), and equilibrium constants are defined accordingly:

$$K_i^j = \frac{c_i^j}{c_i^{N_P*}} = \frac{\Phi_i^{N_P*}}{\Phi_i^j},\quad i = 1, \cdots, N_C,\ j = 1, \cdots, N_P \tag{36}$$

Based on the above definition, the distribution expressions for each component in all phases, including the reference phase N_P*, can be formulated accordingly:

$$c_i^j = \frac{c_i K_i^j}{1 + \sum_{l=1}^{N_P-1} \alpha^l \left(K_i^l - 1\right)},\ i = 1, \cdots, N_C,\ j = 1, \cdots, N_P \tag{37}$$

By combining the above equations and eliminating the reference phase, a unified material balance expression for the distribution of each component across all phases can be derived, commonly known as the Rachford-Rice (R-R) equation:

$$\sum_{i=1}^{N_C} \frac{c_i\left(K_i^j - 1\right)}{1 + \sum_{l=1}^{N_P-1} \alpha^l\left(K_i^l - 1\right)} = 0, \quad j = 1, \cdots, N_P \tag{38}$$

The convergence condition is:

$$r = \sum_{j=1}^{N_P} \sum_{i=1}^{N_C} \left[\frac{F_i^j}{F_i^{N_P*}} - 1\right]^2 \leq 10^{-12} \tag{39}$$

where, F_i^j denotes the fugacity of component i in phase j; Φ_i^j is the fugacity coefficient of component i in phase j; α^j represents the phase fraction of phase j; c_i^j is the mole fraction of component i in phase j; K_i^j is the equilibrium constant of component i between phase j and the reference phase N_P*, defined as the mole fraction ratio $c_i^j/F_i^{N_P*}$; z_i denotes the feed amount of component i; r is the residual used for convergence checking of the flash iteration (Jing, 2020); and N_P is the total number of phases.

In summary, the multiphase flash calculation procedure adopted in this study is as follows:

1) Calculate the initial value of the equilibrium constant and the initial phase fractions are assumed to be uniformly distributed as $1/N_P$;

Table 1
Inlet fluid components (MeOH mass fraction 30% in aqueous phase).

Components	mol%
H_2O	2.200
N_2	1.100
CO_2	0.153
C1	83.868
C2	5.654
C3	2.497
*i*C4	0.584
*n*C4	0.784
*i*C5	0.344
*n*C5	0.220
*n*C6	0.258
*n*C7	0.437
*n*C8	1.059
*n*C9	0.233
*n*C10	0.060
*n*C11	0.020
MeOH	0.527

Table 2
Inlet fluid components (MeOH mass fraction 50% in aqueous phase).

Components	mol%
H_2O	2.185
N_2	1.092
CO_2	0.152
C1	83.277
C2	5.614
C3	2.479
*i*C4	0.579
*n*C4	0.779
*i*C5	0.342
*n*C5	0.218
*n*C6	0.256
*n*C7	0.434
*n*C8	1.052
*n*C9	0.232
*n*C10	0.061
*n*C11	0.021
MeOH	1.228

Table 3
Elevation and distance along the pipeline.

Distance, m	0	2000	4000	6000	8000
Elevation, m	0	350	210	490	280

2) The Rachford-Rice equation (Eq. (34)) is solved using the optimization algorithm proposed by Okuno (Okuno et al., 2010);
3) Phase compositions are updated using Eq. (33);
4) Fugacity coefficients and fugacities of each component in all phases are calculated using the PR-HuronVidal EoS;
5) The fugacity equilibrium criterion is evaluated using Eq. (35). If the convergence criterion is met, the iteration terminates and the phase equilibrium result is obtained. Otherwise, the equilibrium constants are updated based on fugacity coefficients (Eq. (32)), and the process returns to step 2 for further iteration until convergence is achieved according to Eq. (35).

It should be noted that although this paper establishes a steady-state inhibitor tracking model, it can still track changes in inhibitor concentration in the aqueous phase. First, the hydrothermal field (pressure and temperature profiles) and the steady flow variables (e.g., liquid holdup and phase volumetric fractions) are treated as time-invariant, while the overall composition in each pipe section is updated in time to represent the convection-dominated propagation of an inlet composition change. When the fluid composition at the inlet first enters or changes, the overall fluid composition within the pipeline will undergo alteration. To calculate this change and more accurately determine the inhibitor distribution during steady-state conditions, the following computational method is employed in this paper.

(1) Definition of a composition-switching factor.

When the inhibitor concentration changes at time t_s, let z^{old} and z^{new} denote the overall inlet composition vectors before and after an inhibitor dosage change, respectively. For pipe section n, a composition-switching factor $s_n(t) \in [0,1]$ is defined, where $s_n = 0$ indicates that the section still contains the "old" composition and $s_n = 1$ indicates full replacement by the "new" composition. The time grid is $t^m = m\Delta t$. The inlet boundary value is as Eq. (40).

$$s_{in}^m = \begin{cases} 0, & t^m < t_s \\ 1, & t^m \geq t_s \end{cases} \tag{40}$$

(2) Composition update in each section.

For section n, the in-situ aqueous holdup volume and aqueous volumetric flow rate under the steady flow field are defined as Eq. (41).

$$U_{w,n} = A_c \Delta L V_{f,w,n}, \; q_{w,n} = \frac{\dot{m}_{w,n}}{\rho_{w,n}}, \tag{41}$$

where $U_{w,n}$ is aqueous volume in section n, A_c is the cross-sectional area, ΔL is the section length, $V_{f,w,n}$ is the aqueous volume fraction in section n, $\dot{m}_{w,n}$ is the aqueous mass flow rate, and $\rho_{w,n}$ is the aqueous density. The fraction of the section replaced within one time step is as Eq. (42).

$$\xi_n = \min\left(1, \max\left(0, \frac{q_{w,n}\Delta t}{V_{w,n}}\right)\right) \tag{42}$$

The switching factor is marched in time as Eq. (43).

$$s_1^{m+1} = (1-\xi_1)s_1^m + \xi_1 s_{\text{in}}^m$$
$$s_n^{m+1} = (1-\xi_n)s_n^m + \xi_n s_{n-1}^m,\ n = 2,\ldots,N \quad (43)$$

Notably, when the change does not traverse an entire section within one time step ($\xi_n < 1$), only partial replacement occurs and s_n increases gradually rather than switching instantaneously.

(3) Time-dependent overall composition in each section.

The overall composition vector in section n at time t^m is reconstructed by linear mixing as Eq. (44).

$$z_{i,n}^m = (1-s_n^m)z_i^{\text{old}} + s_n^m z_i^{\text{new}} \quad (44)$$

(4) Flash closure for inhibitor partitioning (performed only where composition changes).

Given the steady average pressure and temperature ($P_{\text{avg},n}$, $T_{\text{avg},n}$) of each pipe section, a three-phase flash calculation is performed using z_n^m as the feed to obtain phase fractions and phase compositions, from which the inhibitor mole fraction in the aqueous phase is extracted. Since flash calculations are the most time-consuming part, they are only recomputed for sections in the transition zone. For sections where s_n^m is sufficiently close to 0 or 1, the corresponding steady flash results using z^{old} or z^{new} are reused.

(5) Time-step selection.

To ensure numerical stability and physical consistency of the upwind update, the time step is chosen to satisfy $\xi_n \leq 1$ for all sections, i.e., $\Delta t \leq \min_n (U_{\text{w},n}/q_{\text{w},n})$. In practical calculations, a smaller Δt can be selected to better resolve sharp composition fronts.

3. Results and discussion

In engineering practice, the mass concentration of thermodynamic inhibitors as hydrate inhibitors is generally 20%–50% (Huang, 2011). Two mass concentrations of 30% and 50% are chosen for the calculations in this paper.

The examples used in this part are typical components in deep-sea oil and gas fields, which can reflect the phase behavior and flow characteristics of fluids in deep-sea environments, and are suitable for the study of hydrate inhibition under high-pressure and low-temperature conditions in the deep sea.

3.1. Case details

(1) Simulation Case 1

In simulation example 1, the specific parameters include pipeline inlet fluid pressure, temperature, component composition, mass flow rate, pipeline diameter, internal diameter, elevation profile along the pipeline, ambient temperature, total heat transfer coefficient, and other key factors. Additionally, MeOH is present in the aqueous phase with mass fractions of 30% and 50%, respectively. The detailed values for these parameters are presented in Tables 1–4.

(2) Simulation Case 2

Without altering the other parameters of the pipeline, the MeOH in the inlet fluid composition is replaced with MEG, with mass fractions in the aqueous phase of 30% and 50%, respectively. The detailed data for these cases are presented in Tables 5 and 6.

3.2. Comparative analysis of results

(1) Simulation Case 1

Figs. 4 and 5 compare the distribution of pressure, temperature, and inhibitor concentration obtained by this model and OLGA along the pipeline for MeOH mass fractions of 30% and 50%,

Table 5
Inlet fluid components (MEG mass fraction 30% in aqueous phase).

Components	mol%
H_2O	2.311
N_2	1.101
CO_2	0.154
C1	83.965
C2	5.660
C3	2.500
*i*C4	0.586
*n*C4	0.788
*i*C5	0.346
*n*C5	0.221
*n*C6	0.260
*n*C7	0.439
*n*C8	1.064
*n*C9	0.235
*n*C10	0.061
*n*C11	0.020
MEG	0.288

Table 6
Inlet fluid components (MEG mass fraction 50% in aqueous phase).

Components	mol%
H_2O	2.303
N_2	1.097
CO_2	0.153
C1	83.645
C2	5.639
C3	2.490
*i*C4	0.584
*n*C4	0.785
*i*C5	0.345
*n*C5	0.220
*n*C6	0.259
*n*C7	0.438
*n*C8	1.060
*n*C9	0.234
*n*C10	0.060
*n*C11	0.020
MEG	0.667

Table 4
Pipe parameters.

Inner diameter, m	Diameter, m	Inlet temperature, K	Inlet pressure, MPa	Mass flow rate, kg/s	Ambient temperature, K	Total heat transfer coefficient, W/(m²·K)
0.1337	0.154	306.15	9.962	4.726	277.15	2.28

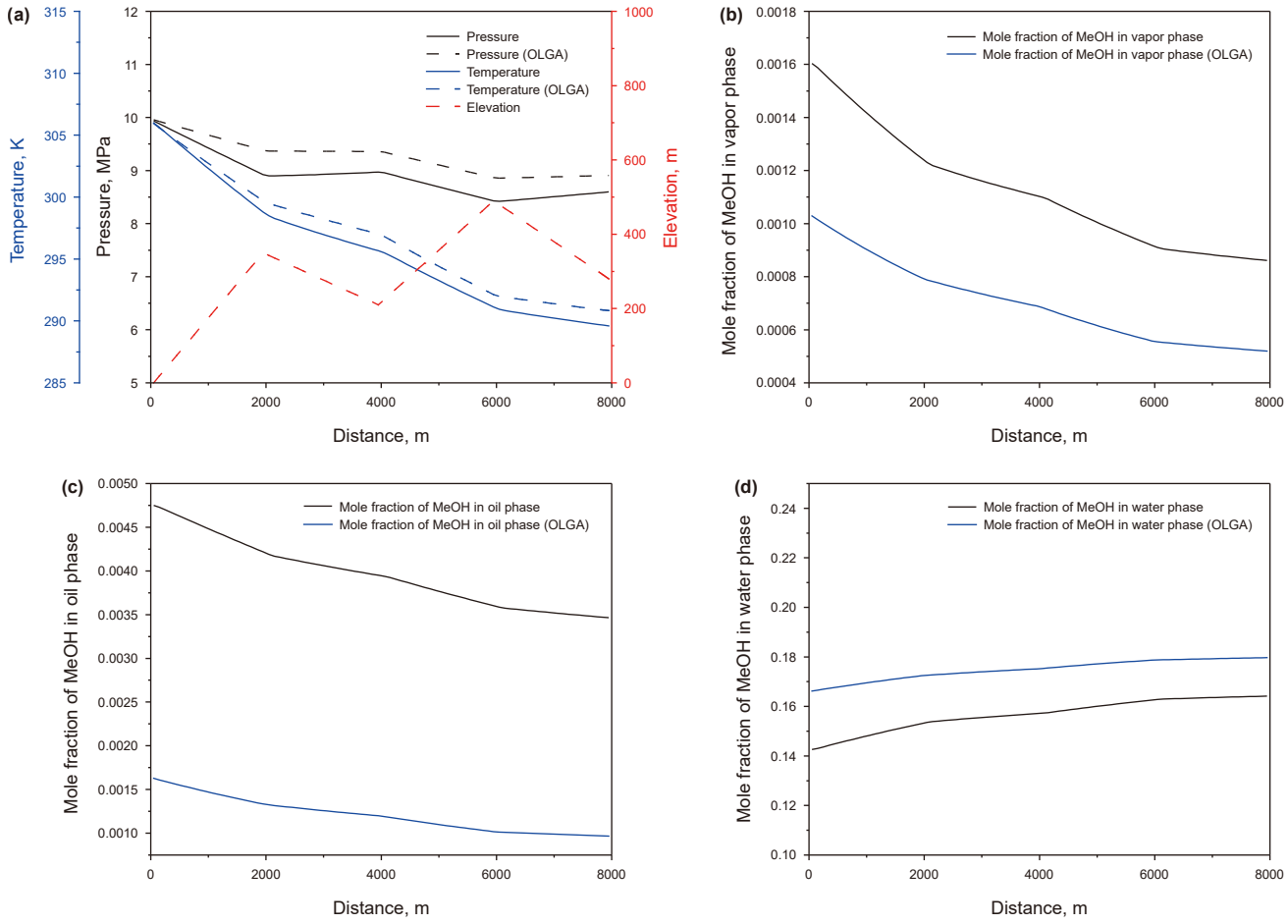

Fig. 4. Comparison results at MeOH mass fraction 30%. **(a)** Pipeline pressure distribution and temperature distribution (MeOH mass fraction 30%). **(b)** Mole fraction of MeOH in vapor phase (MeOH mass fraction 30%). **(c)** Mole fraction of MeOH in oil phase (MeOH mass fraction 30%). **(d)** Mole fraction of MeOH in water phase (MeOH mass fraction 30%).

respectively. Both the 30% and 50% MeOH concentration simulations show consistent trends between the two models, though some discrepancies in specific values are observed.

For both MeOH concentrations (Figs. 4(a) and 5(a)), the pressure and temperature distribution at the outlet calculated by this work are slightly lower than those computed by OLGA. At a MeOH mass fraction of 30%, the average errors in pressure and temperature are 3.98% and 0.33%, respectively. At a MeOH mass fraction of 50%, the average errors are 1.26% for pressure and 0.17% for temperature. In the middle section of the pipeline, the pressure trend calculated by this work aligns with OLGA's results when accounting for elevation, though the overall pressure values are lower. This discrepancy arises from different modeling assumptions: OLGA employs a two-fluid model and reaches steady-state results after convergence, while this work uses a simplified steady-state model, leading to more conservative pressure estimates along the pipeline.

Figs. 4 (b)–(d) and 5 (b)–(d) illustrate the inhibitor distribution in the gas, oil, and aqueous phases under both MeOH concentrations. The MeOH concentrations in the gas and oil phases calculated by this work are higher than OLGA's results, while the concentrations in the aqueous phase are lower. The discrepancies in MeOH concentration between the two models are 10.43% and 8.66%, respectively. The discrepancy in inhibitor concentration in the aqueous phase primarily arises from the differences in how inhibitor distribution is modeled in this study compared to OLGA. Specifically, OLGA's hydrate inhibitor tracking module does not consider the dissolution of hydrocarbon components into the aqueous phase, which can lead to an overestimation of inhibitor concentration in water. Moreover, OLGA determines component distribution based on pre-generated PVT tables, which are generated by its built-in Multiflash software but does not employ its phase equilibrium flash calculation module. Although the Multiflash software itself is capable of performing multiphase flash calculations, this functionality is not employed when calculating inhibitor distribution. In contrast, the present model applies a section-wise flash calculation using the PR EoS with the HuronVidal mixing rule, enabling accurate and thermodynamically consistent prediction of inhibitor partitioning among all three phases. Overall, the MeOH concentration in the aqueous phase calculated by this work is more conservative, which offers greater safety in practical applications.

(2) Simulation Case 2

Figs. 6 and 7 compare the distribution of pressure, temperature, and inhibitor concentration in the pipeline for MEG mass fractions of 30% and 50%, respectively, as simulated by this work and OLGA. Overall, for both MEG concentrations, the calculation results from this work demonstrate better consistency in trend with OLGA compared to the MeOH inhibitor results.

Under the conditions of both MEG concentrations (Figs. 6(a) and 7(a)), for a 30% MEG mass fraction, the average error in pressure is 4.45%, and 0.38% for temperature. For a 50% MEG mass

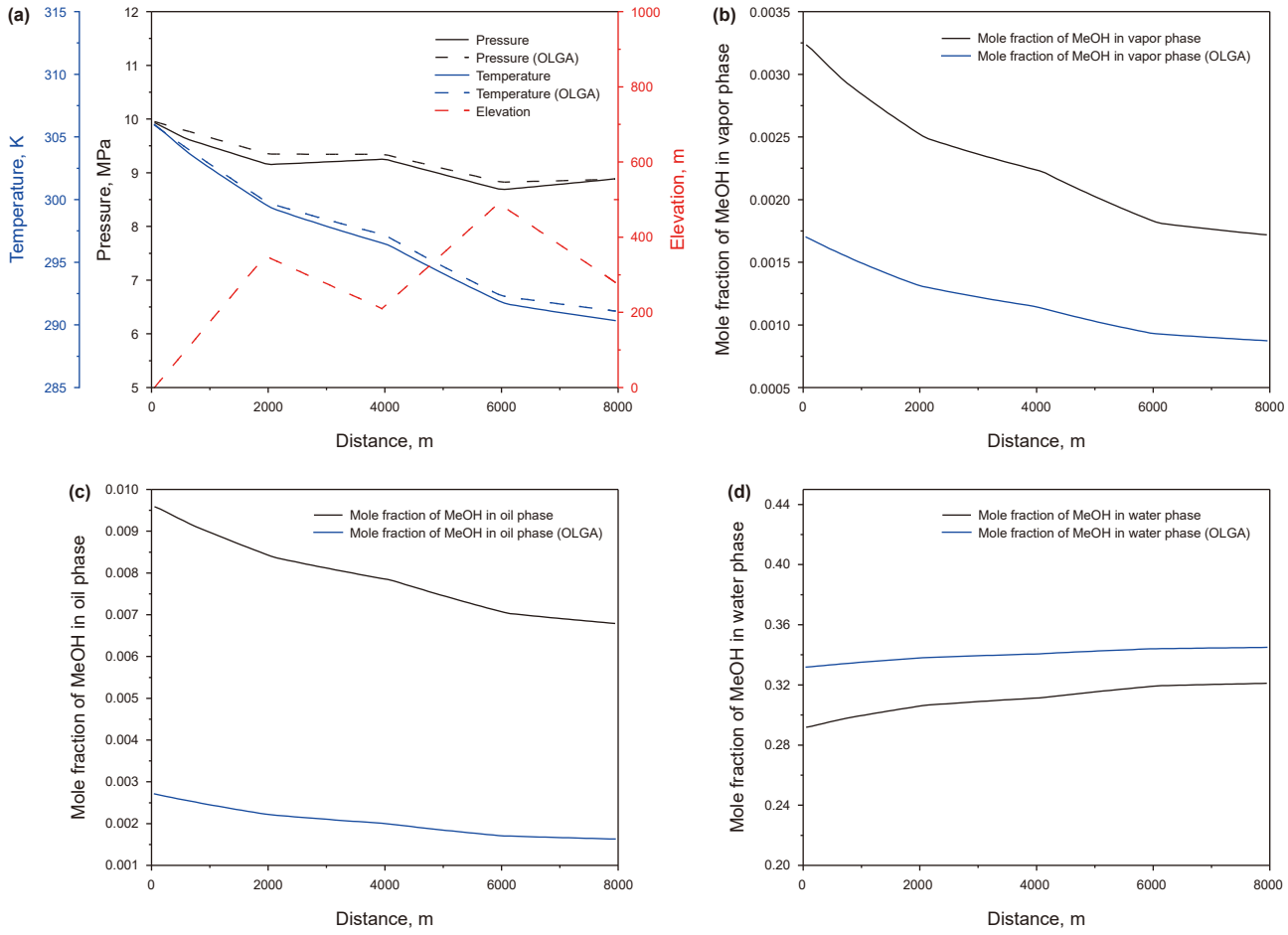

Fig. 5. Comparison results at MeOH mass fraction 50%. **(a)** Pipeline pressure distribution and temperature distribution (MeOH mass fraction 50%). **(b)** Mole fraction of MeOH in vapor phase (MeOH mass fraction 50%). **(c)** Mole fraction of MeOH in oil phase (MeOH mass fraction 50%). **(d)** Mole fraction of MeOH in water phase (MeOH mass fraction 50%).

fraction, the average errors are 3.58% for pressure and 0.41 % for temperature. In the middle section of the pipeline, however, the calculated results are lower than those of OLGA due to differences in modeling, though the overall trend remains consistent with OLGA's calculations.

Figs. 6(b)–(d) and 7(b)–(d) illustrate the inhibitor distribution in the gas, oil, and aqueous phases under the two MEG concentrations. Although the molar fraction of MEG in the gas and oil phases calculated by this work is still higher than OLGA's results, its significantly lower solubility in these phases compared to MeOH means its effect in practical pipeline applications can be disregarded. Therefore, focus should be placed on the molar fraction of MEG in the aqueous phase. The simulation results show that the distribution in the aqueous phase under both MEG concentrations differs from OLGA by only 0.02% and 0.11%, respectively, indicating a high level of consistency between the two models.

In summary, the proposed hydrate inhibitor tracking model was compared with the widely used OLGA software, focusing on the distribution of inhibitors such as MeOH and MEG along the pipeline. Both models showed similar trends in inhibitor distribution, indicating a strong overall agreement. However, for MeOH, a difference of approximately 10% was observed in the distribution calculations between the two models. While not particularly significant, this discrepancy is worth noting.

The source of this slight difference may be due to OLGA's use of the Multiflash phase equilibrium software, which handles gas-liquid phase equilibria differently from the flashing calculations employed in our model. Although the overall trends are consistent, variations in phase behavior modeling and parameter settings could cause minor differences in MeOH phase compositions under specific pressure and temperature conditions.

In addition, OLGA's built-in multiphase flow model is a highly detailed three-phase system that calculates oil, gas, and water flows in a given pipeline configuration. In contrast, our model is derived based on the Beggs-Brill method, which may not achieve the same accuracy in some flow regimes (e.g., stratified or slug flow). These differences in flow modeling may account for the 10% difference in MeOH distribution, especially in areas where the flow transition is more pronounced.

Despite these minor differences, the overall agreement between the two models confirms the reliability of the methodology presented in this paper. The 10% difference highlights areas for future improvements, such as refining the multiphase flow models and incorporating more detailed interphase behavior (e.g., phase transitions and interfacial dynamics (Qi et al., 2023; Song et al., 2023). Addressing these aspects would further enhance the accuracy of inhibitor distribution predictions under varying pipeline conditions.

3.3. Sensitivity analysis

To evaluate the adaptability of the proposed steady-state inhibitor tracking model, a series of sensitivity analyses are conducted. These analyses aim to quantify how variations in key

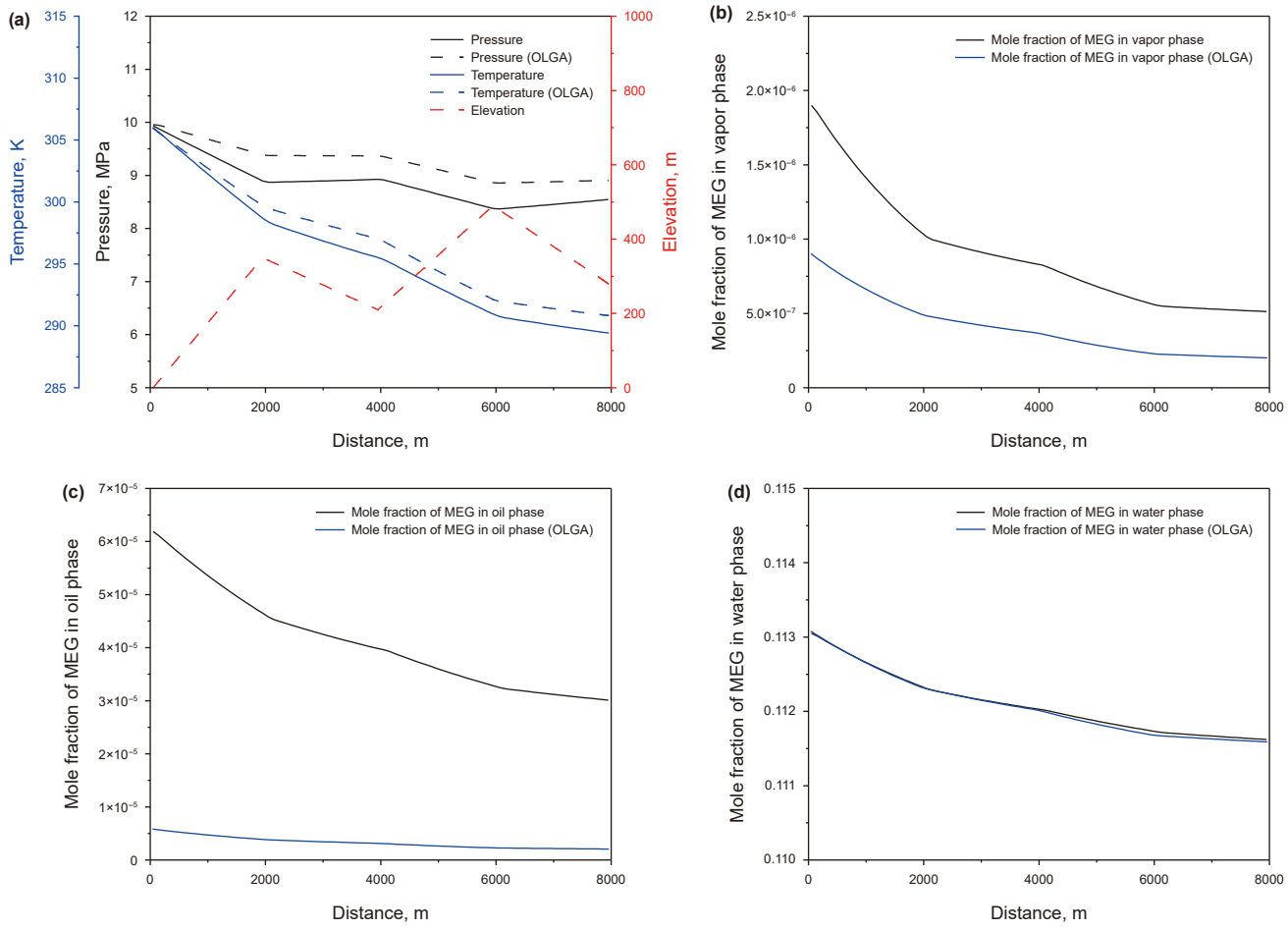

Fig. 6. Comparison results at MEG mass fraction 30%. **(a)** Pipeline pressure distribution and temperature distribution (MEG mass fraction 30%). **(b)** Mole fraction of MEG in vapor phase (MEG mass fraction 30%). **(c)** Mole fraction of MEG in oil phase (MEG mass fraction 30%). **(d)** Mole fraction of MEG in water phase (MEG mass fraction 30%).

physical and model parameters affect the prediction of pressure, temperature, and inhibitor distribution along the pipeline. In particular, we focus on terrain configuration, external heat transfer conditions, and phase equilibrium algorithms, as they are closely linked to the thermal-hydraulic behavior of multiphase flow and the partitioning of inhibitors. The objective is to identify the dominant influencing factors, assess the generalizability of the model under varying operational conditions, and provide guidance for model selection and parameter setting in practical applications.

3.3.1. Pipeline terrain variations

To evaluate the applicability of the steady-state model under different terrain conditions, we introduced two additional pipeline terrains. These include one with a steep slope and another with a riser. The detailed data are presented in the tables below.

The pipeline parameters remain consistent with cases in Section 3.1, and the fluid composition is set as a 30% MeOH mass fraction in the aqueous phase. In the main modeling framework, the Beggs-Brill model is adopted for steady-state pressure drop calculations to align with mainstream industrial practices. However, considering that the Beggs-Brill model has known limitations under certain flow regimes, such as slug flow or highly inclined sections, we additionally introduce the Unified model and the Mukherjee-Brill model in the sensitivity analysis. These models, which offer improved physical consistency and wider applicability, are used to compare and evaluate how different steady-state flow models affect the predicted inhibitor distribution. The results are presented in Fig. 8.

The Mukherjee-Brill model (Mukherjee and Brill, 1985) builds upon the Beggs-Brill model by modifying correlations for inclined and vertical pipe sections. It enhances prediction accuracy under moderately inclined conditions and, compared to the Beggs-Brill model, performs better in handling flow pattern transitions, particularly in pulsating and annular flow regimes. However, it still relies on empirical flow pattern maps and discrete transitions.

The Unified model (Zhang et al., 2003) is a mechanistic flow model based on continuous equations that can predict flow behavior under all flow regimes. It eliminates the need for manual switching between flow patterns and ensures better physical consistency, especially in systems with large elevation changes or fluctuating gas-liquid ratios (GLRs). In this study, it is introduced in the sensitivity analysis to assess the impact of more advanced hydraulic models on the prediction of inhibitor distribution.

The computational results show that under the terrain conditions of Case 1 (pipe inclination less than 15°), all three models produce results with small deviations from those calculated by OLGA. The average relative deviation along the pipeline for all three models is less than 3%, indicating that the Beggs-Brill, Mukherjee-Brill, and Unified models are well-suited for pipelines with mild terrain variation.

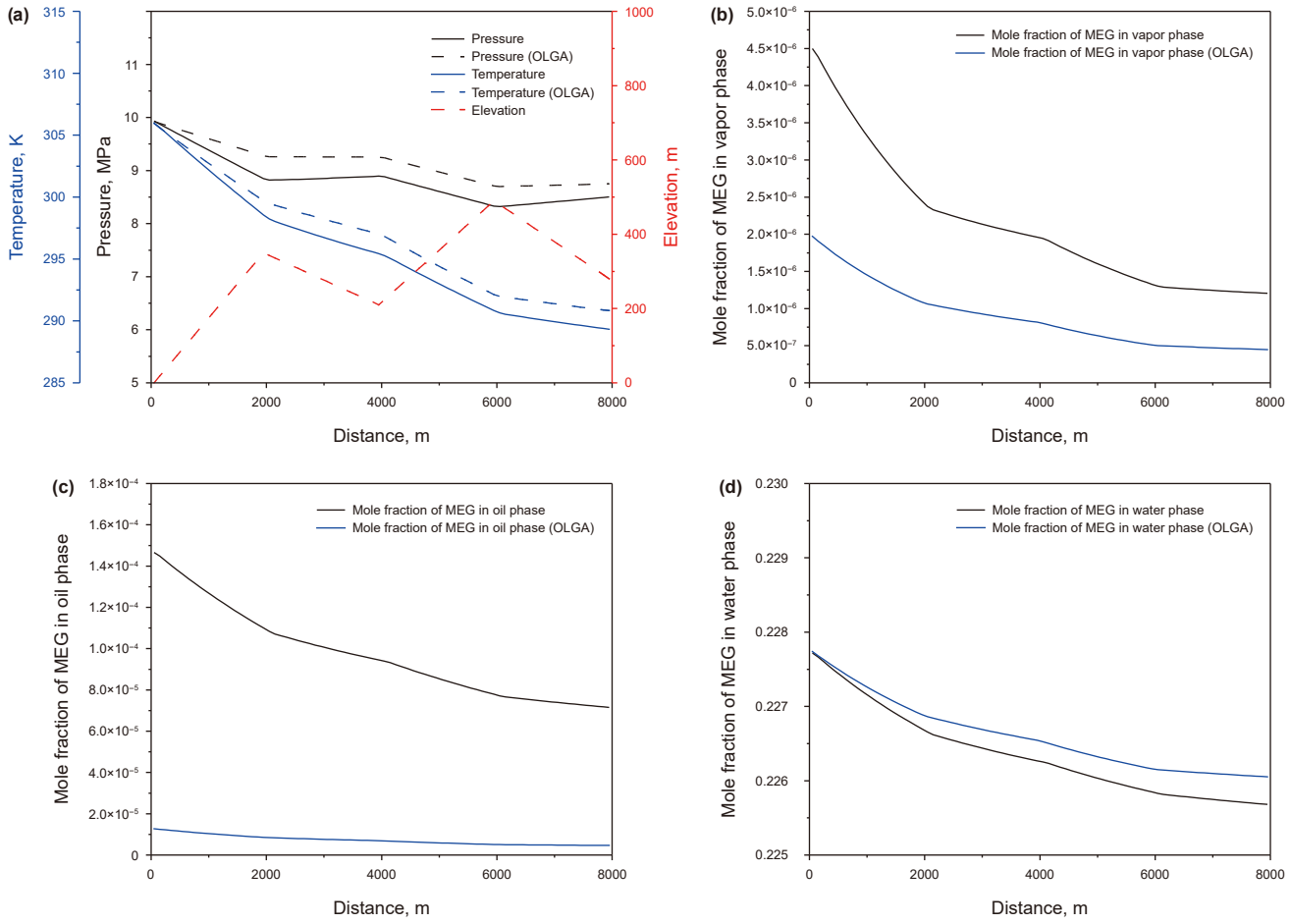

Fig. 7. Comparison results at MEG mass fraction 50%. **(a)** Pipeline pressure distribution and temperature distribution (MEG mass fraction 50%). **(b)** Mole fraction of MEG in vapor phase (MEG mass fraction 50%). **(c)** Mole fraction of MEG in oil phase (MEG mass fraction 50%). **(d)** Mole fraction of MEG in water phase (MEG mass fraction 50%).

Under the terrain conditions of Case 2 (pipe inclination of 45°), the Beggs-Brill model still maintains the general trend seen in OLGA but exhibits a larger deviation, with an average relative error of 14.3%. In contrast, the Mukherjee-Brill and Unified models maintain average relative errors below 2.5%, indicating that the Beggs-Brill model is no longer suitable for large-inclination scenarios.

In Case 3, which includes a vertical riser section, the average relative deviation between the Beggs-Brill model and OLGA is 7.0%, while the Mukherjee-Brill model shows a deviation of 1.3%, and the Unified model only 0.5%.

This sensitivity analysis demonstrates that different steady-state multiphase flow models lead to varying predictions of pressure distribution along the pipeline, which in turn affects phase equilibrium conditions and the resulting inhibitor distribution. For pipelines with relatively flat terrain, the Beggs-Brill, Mukherjee-Brill, and Unified models can all reasonably reproduce the trends predicted by OLGA, with acceptable engineering accuracy. However, in cases involving steep inclines or vertical risers, the Beggs-Brill model exhibits a significant drop in accuracy, while the Mukherjee-Brill model offers moderate adaptability. The Unified model consistently aligns closely with OLGA across all terrain types. These results confirm that the proposed simulation model is flexible and compatible with different steady-state models and also indicate the importance of selecting an appropriate flow model based on terrain complexity to ensure reliable pressure and temperature predictions in engineering applications.

3.3.2. *Ambient temperature and heat transfer coefficient variations*

In steady-state pipeline simulations, external heat transfer conditions are key factors influencing the temperature distribution along the pipeline, thereby affecting local thermal conditions and phase equilibrium results obtained from flash calculations. Common boundary parameters for thermal exchange include the overall heat transfer coefficient and ambient temperature. This sensitivity analysis separately examines the effects of varying ambient temperature and overall heat transfer coefficient.

The pipeline parameters used in this section are consistent with cases in Section 3.1. The Unified model, which has demonstrated broader applicability, is employed for the steady-state simulation. Since the temperature drop model used in this section is independent of pipeline inclination, only the terrain profile shown in Table 7 is considered for analysis (see Tables 8 and 9).

The ambient temperatures are set to 277.15, 285.15, and 293.15 K, while the overall heat transfer coefficients are set to 1, 2.28, and 5 W/(m^2·K). The corresponding simulation results for temperature are shown in Figs. 9(a) and 10(a), and the MeOH concentration distribution in the aqueous phase is presented in Figs. 9(b) and 10(b).

The simulation results indicate that under the terrain profile of Case 1, the deviations between the calculated temperature results and those from OLGA are minor for both ambient temperature and heat transfer coefficient variations, with highly consistent trends. For ambient temperature changes, the average relative deviation along the pipeline under all three temperature settings is less than

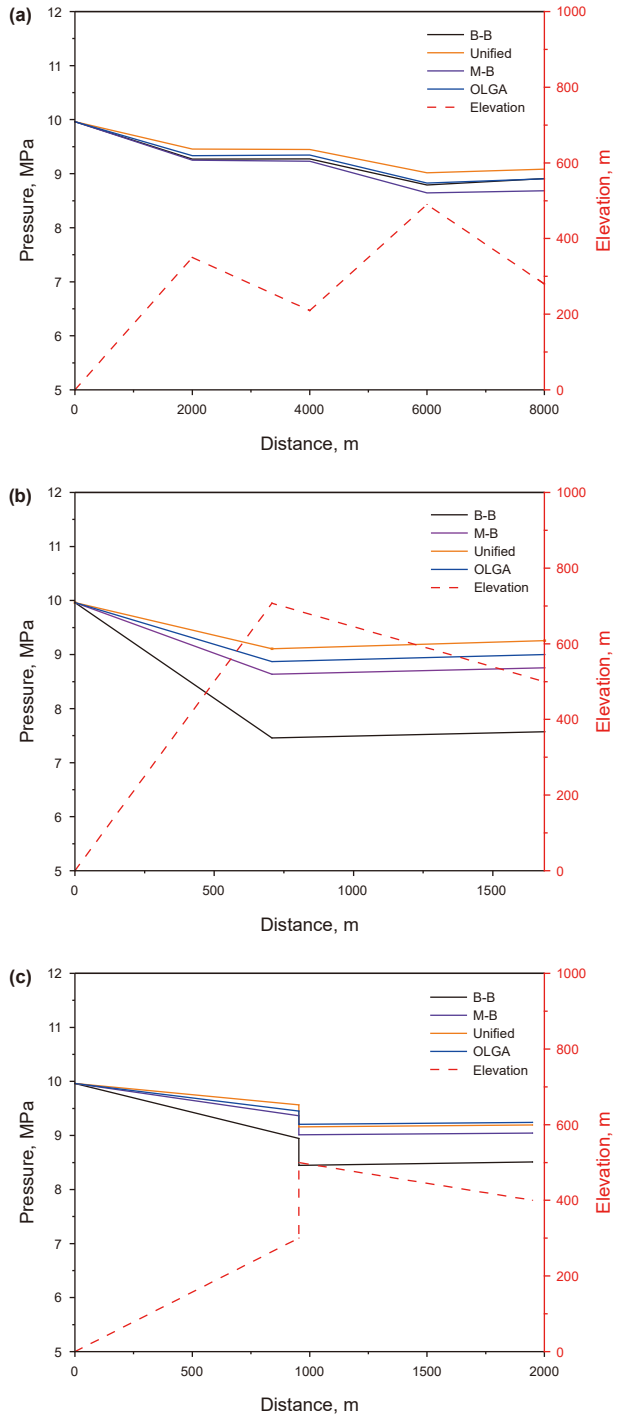

Fig. 8. Pipeline pressure distribution at different terrains. **(a)** Pipeline pressure distribution (gentle slope, <15°; MeOH mass fraction 30%). **(b)** Pipeline pressure distribution (steep slope, 45°; MeOH mass fraction 30%). **(c)** Pipeline pressure distribution (including riser; MeOH mass fraction 30%).

Table 7
Pipeline terrain 1 (gentle slope, <15°).

Distance, m	0	2000	4000	6000	8000
Elevation, m	0	350	210	490	280

1%, with a maximum absolute error of 1.86 K. Similarly, for changes in the heat transfer coefficient, the average relative deviation remains below 1%, and the maximum absolute error is 1.92 K. These

Table 8
Pipeline terrain 2 (steep slope, 45°).

Distance, m	0	1000	2000
Elevation, m	0	707	500

Table 9
Pipeline terrain 3 (including riser).

Distance, m	0	1000	0	2000
Elevation, m	0	300	500	400

results demonstrate that the temperature distribution model employed in this study is robust and applicable to different thermal boundary conditions.

As shown in Figs. 9(b) and 10(b), the predicted distributions of MeOH in the aqueous phase also closely match those computed by OLGA across all thermal conditions. As the temperature decreases, the vapor pressure of MeOH declines, resulting in a higher concentration retained in the aqueous phase. Moreover, the deviations between our method and OLGA remain largely unaffected by variations in ambient temperature and heat transfer coefficient. This indicates that while temperature is a critical factor influencing inhibitor distribution, it is not the primary source of deviation between this study and OLGA results.

3.3.3. Flash module variations

To quantify the impact of equilibrium algorithm differences on prediction accuracy, we conducted a sensitivity analysis by comparing different flash calculation modules from commercial software. Although variations in fluid composition can indeed influence the phase distribution of inhibitors, the steady-state inhibitor distribution in this study is determined via multiphase flash calculations, which are highly dependent on the underlying phase equilibrium model. Therefore, rather than altering fluid composition, comparing different flash calculation modules offers a more direct and accurate means of evaluating the predictive performance and applicability of the thermodynamic algorithms themselves. This approach also highlights the structural robustness and sensitivity of the proposed model at the model level.

Accordingly, we selected PVTsim (Version: Nova 5.3) and Multiflash (Version: 7.3) as representative commercial tools for comparison. Using the four case studies from Section 3.1, the pipeline parameters were kept consistent. The steady-state temperature and pressure results along the pipeline were first computed using our model, followed by inhibitor distribution calculations using the flash modules in PVTsim and Multiflash. For consistency, the PR-HuronVidal EoS is employed across all flash calculations. The results are shown in Figs. 11 and 12.

Based on the above simulation results, for both MeOH concentrations (mass fractions 30% and 50%), the results obtained in this study are highly consistent with those calculated by PVTsim. Specifically, the average deviation for the 30% MeOH case is 0.17%, and for the 50% case, the average deviation is 0.12%. In contrast, the deviations from Multiflash are 5.95% and 4.96%, respectively. For MeOH, as the pipeline temperature decreases along its length, the MeOH concentration in the aqueous phase increases continuously. This is because the vapor pressure of MeOH decreases with decreasing temperature, causing MeOH in the vapor phase to dissolve into the aqueous phase and raise its concentration.

In OLGA's inhibitor tracking module, rigorous phase equilibrium flash calculations are not applied. Instead, the partial pressure of MeOH in the vapor phase is directly taken as its concentration, which is then used to adjust its concentration in the

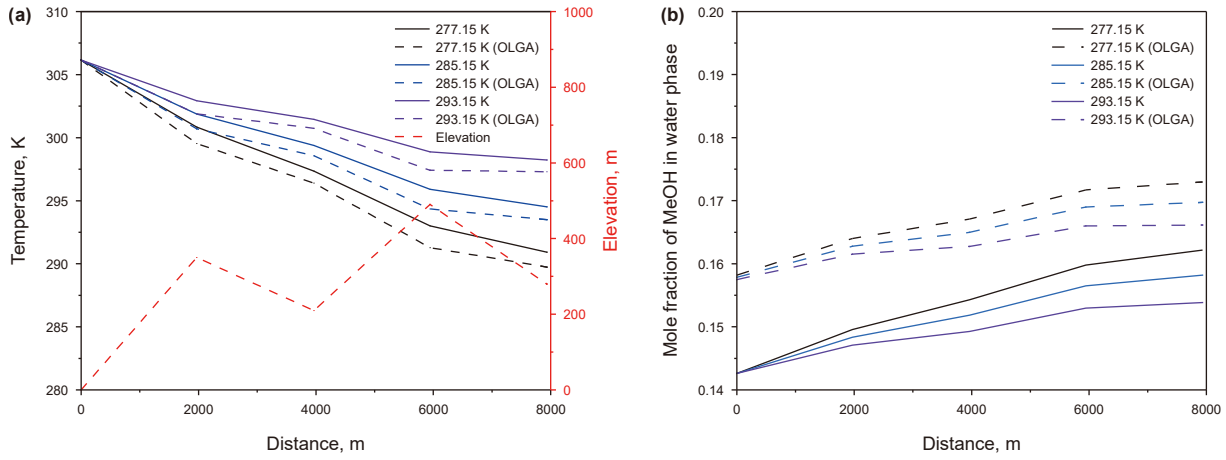

Fig. 9. Pipeline temperature distribution and mole fraction of MeOH in water phase at different ambient temperatures. **(a)** Pipeline temperature distribution at different ambient temperatures (Gentle slope, <15°; MeOH mass fraction 30%). **(b)** Mole fraction of MeOH in water phase at different ambient temperatures (Gentle slope, <15°; MeOH mass fraction 30%).

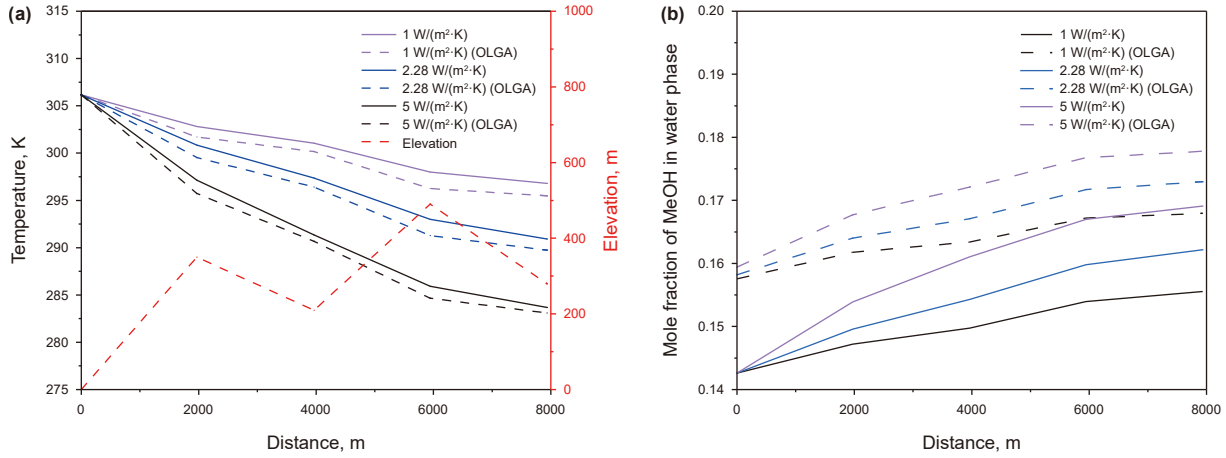

Fig. 10. Pipeline temperature distribution and mole fraction of MeOH in water phase at different total heat transfer coefficients. **(a)** Pipeline temperature distribution at different total heat transfer coefficients (gentle slope, <15°; MeOH mass fraction 30%). **(b)** Mole fraction of MeOH in water phase at different total heat transfer coefficients (gentle slope, <15°; MeOH mass fraction 30%).

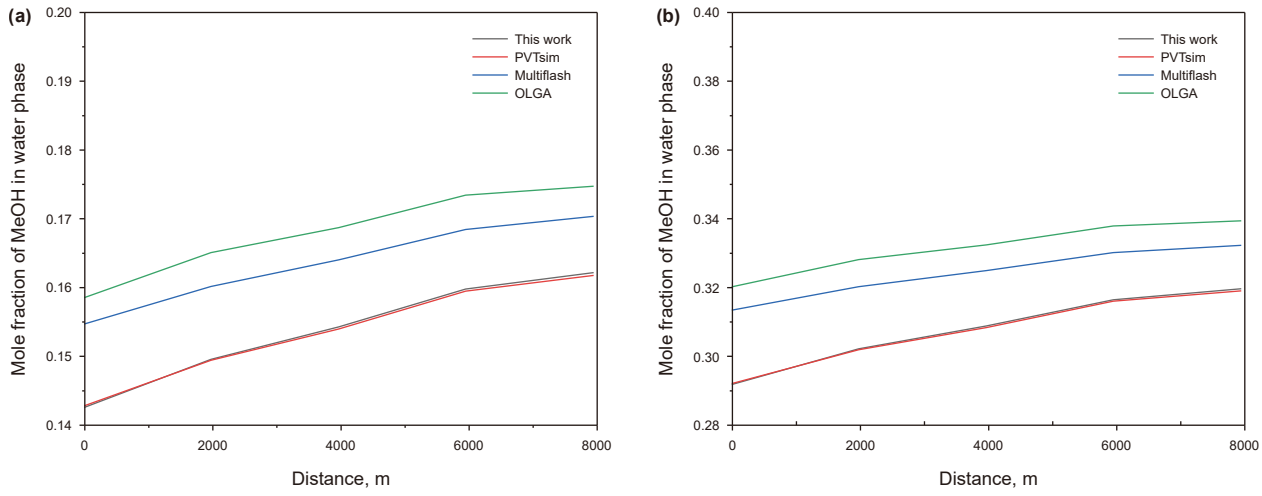

Fig. 11. Flash module results comparison at different MEG concentrations. **(a)** Mole fraction of MeOH in water phase (MeOH mass fraction 30%). **(b)** Mole fraction of MeOH in water phase (MeOH mass fraction 50%).

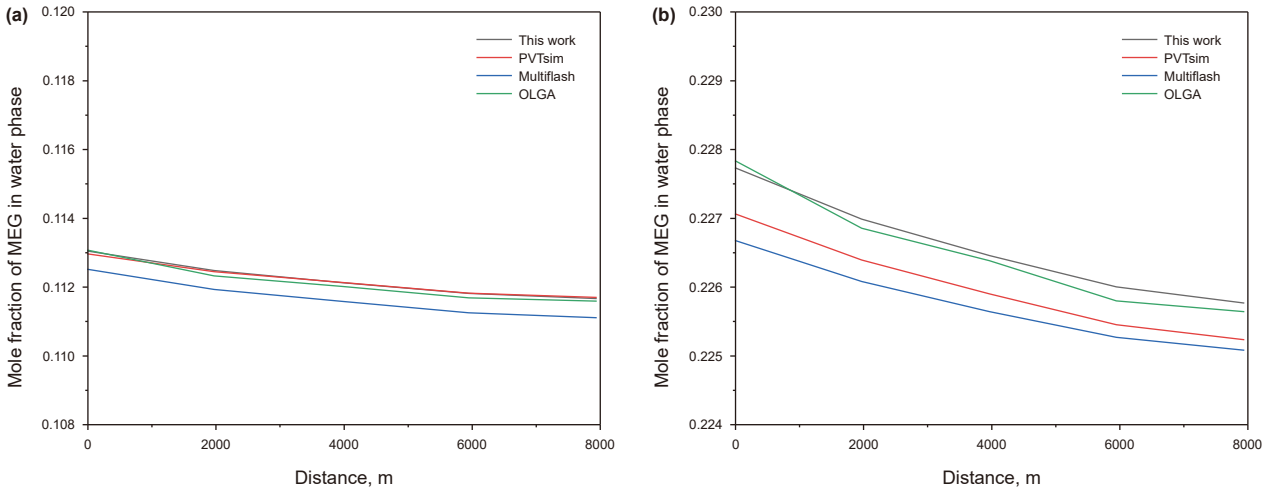

Fig. 12. Flash module results comparison at different MEG concentrations. **(a)** Mole fraction of MEG in water phase (MEG mass fraction 30%). **(b)** Mole fraction of MEG in water phase (MEG mass fraction 50%).

aqueous phase. Additionally, OLGA does not consider the distribution of oil in the aqueous phase, effectively treating the aqueous phase as consisting only of water and inhibitor. These simplifications may lead to an overestimation of the MeOH content in the aqueous phase calculated by OLGA. The discrepancy between Multiflash and this study may also arise from differences in the binary interaction parameters used in the EoS.

For MEG, as the pipeline temperature decreases along its length, the concentration of MEG in the aqueous phase shows a decreasing trend. This is because MEG has an extremely low vapor pressure and exists in only trace amounts in the gas phase, significantly lower than the vapor pressure of water. As a result, water vapor gradually condenses into the aqueous phase with falling temperature, thereby diluting the MEG concentration. Since the vapor-phase loss of MEG is negligible, the results from OLGA's simplified calculation method are very close to those obtained from the rigorous flash calculation method used in this study. Furthermore, the average relative deviations between this study's results and those of PVTsim and Multiflash are both within 0.5%, indicating that the proposed method yields highly accurate predictions for the distribution of MEG in the aqueous phase.

Based on all the above sensitivity analyses, it can be concluded that under the selected steady-state hydraulic and thermal models, the most critical factor affecting the distribution of inhibitors in the aqueous phase is the phase equilibrium calculation. For MeOH, due to its relatively high vapor phase loss and the assumptions and simplifications in OLGA's hydrate inhibitor tracking model, there is a noticeable discrepancy of approximately 10%, compared to the results of this study. In contrast, for MEG, which exhibits minimal vapor-phase loss, the phase equilibrium results calculated in this study show good agreement with those obtained from OLGA and other commercial software.

4. Conclusions

The proposed model offers a flexible and efficient solution for tracking hydrate inhibitors in oil-gas-water three-phase flow systems. Due to the complexity of real-world three-phase flow, no single hydraulic model can be universally applied. Therefore, our model allows for the flexible replacement of key components, such as the hydraulic and thermal models, adapting to different pipeline configurations and flow conditions. Crucially, by employing reasonable assumptions and implementing detailed three-phase flash calculations for inhibitor distribution, this approach balances computational efficiency with result accuracy. The resulting inhibitor distribution yields greater precision than commercial software. The specific conclusions are as follows:

(1) The steady-state pressure and temperature results are highly consistent with those calculated by OLGA, with average deviations below 5%, confirming the reliability of the thermal-hydraulic module.
(2) Due to model assumptions in OLGA, the predicted MeOH distribution shows slight deviation but remains generally consistent. The MEG results show excellent agreement, demonstrating strong engineering applicability.
(3) In pipeline cases with significant terrain variation, the Beggs-Brill model and OLGA show larger calculation deviations. However, the proposed model allows flexible replacement of the steady-state pressure model, enabling better adaptability.
(4) The developed flash module is compared with PVTsim and Multiflash. The results align closely with PVTsim, while minor deviations are observed with Multiflash, validating the robustness of the implemented phase equilibrium calculation.

In conclusion, the proposed model enables accurate and flexible prediction of inhibitor distribution under complex multiphase conditions. Under steady-state flow conditions, it can provide a reference for predicting inhibitor distribution inside pipelines, thereby reducing engineering operation and maintenance costs. Future work will focus on incorporating transient effects and further improving the accuracy of phase-specific inhibitor tracking under varying flow and composition scenarios.

CRediT authorship contribution statement

Shang-Fei Song: Writing – review & editing, Writing – original draft, Supervision, Resources, Project administration, Funding acquisition, Formal analysis. **Jia-Hao Yu:** Writing – review & editing, Writing – original draft, Visualization, Validation, Methodology, Investigation, Formal analysis, Data curation. **Yan-Bo Li:** Methodology, Conceptualization. **Hao-Qi Chen:** Resources, Methodology. **Da-Qian Liu:** Writing – review & editing, Formal analysis. **Xiang-Ying Shan:** Writing – review & editing, Formal analysis.

Hai-Hong Chen: Software, Resources. **Hai-Yuan Yao:** Software, Resources. **Bo-Hui Shi:** Supervision, Funding acquisition. **Jing Gong:** Supervision, Resources, Project administration.

Conflict of interest statement

The authors declare no competing interests.

Acknowledgement

This work is supported by Oil & Gas Major Project (Grant Nos. 2025ZD1403004, 2025ZD1403706, 2025ZD1403501), National Natural Science Foundation of China (Grant No. 52574091), Beijing Nova Program (No. 20240484721), all of which are gratefully acknowledged.

Nomenclature

Symbol	Meaning	Units
P	Pressure	Pa
T	Temperature	K
L	Distance of axial flow	m
g	Local gravitational acceleration	m/s^2
u	Velocity	m/s
H	Elevation	m
ρ	Density	kg/m^3
θ	Pipe section inclination	degree
d	Pipeline diameter	m
f	Friction factor	/
W_f	Irreversible frictional losses	m^2/s^2
G	Mass flux rates	kg/(s·m^2)
u_{sg}	Superficial gas velocity	m/s
F_{el}, F_{acc}, F_f	Pressure gradient due to elevation, acceleration and friction	Pa/m
Z	Compression factor	/
P_s	Inlet pressure of pipe sections	Pa
P_e	Outlet pressure of pipe sections	Pa
T_s	Inlet temperature of pipe sections	K
T_e	Outlet temperature of pipe sections	K
T_a	Ambient temperature	K
X_{wg}	Gas phase mass fraction	/
x	Mole fraction of any component	/
C_p	Specific heat capacity of mixture fluids at constant pressure	kJ/(kg·K)
M	Mass flow rate of the gas-liquid mixture	kg/s
D_i	Joule-Thomson coefficient of component i	K/Pa
k	Overall heat transfer coefficient	W/(m^2·K)
i	Hydraulic gradient of liquid phase	m/m
A	Parameter in thermal model	m^{-1}
B	Parameter in thermal model	K
H_L	Liquid holdup	/
λ	Input liquid content	/
q	In-situ volumetric flow rate	m^3/s
μ	Viscosity	Pa·s
V	Mole volume	m^3/mol
V_f	Volume fraction	/
EoS	Equation of state	/
a	Parameter in EoS	Pa·m^6/mol^2
b	Parameter in EoS	m^3/mol
c	Mole fraction of component in any phase	/
α	Phase fraction	/
z	Mole fraction of feed component	/
F	Fugacity	Pa
ϕ	Fugacity coefficient	/
K	Equilibrium constant	/
s	Composition-switching factor	/
t	Time	s
U	Volume	m^3
A_c	Cross-sectional area	m^2
ξ	Replacement ratio	/
$\dot{m}$	Mass flow rate	kg/s

Subscripts/ superscripts	Meaning	Units
g	Gas phase	
L	Liquid phase	
w	Aqueous phase	
i,j,k,l	Index for any component or phase	
n	Pipe section index	
m	Time-step index	
avg	Average	
in	Inlet	
ns	No-slip	

Supplementary data

Supplementary data to this article can be found online at https://doi.org/10.1016/j.petsci.2026.02.015.

References

Alavi, F., Sharifzadeh, M., 2024. Customized federated kernel regression learning for predicting natural gas hydrate equilibrium with thermodynamic inhibitors: A comprehensive study. Chem. Eng. J. 498, 155664. https://doi.org/10.1016/j.cej.2024.155664.

Aman, Z.M., 2021. Hydrate risk management in gas transmission lines. Energy Fuel. 35 (18), 14265–14282. https://doi.org/10.1021/acs.energyfuels.1c01853.

Bakhtyari, A., Rasoolzadeh, A., Mehrabi, K., Javanmardi, J., Mofarahi, M., Nasrifar, K., 2024. Natural gas thermodynamic hydrate inhibitors. In: Advances in Natural Gas: Formation, Processing, and Applications, vol. 3. Natural Gas Hydrates. Elsevier, pp. 233–277. https://doi.org/10.1016/B978-0-443-19219-7.00003-5.

Beggs, D.H., Brill, J.P., 1973. A study of two-phase flow in inclined pipes. J. Petrol. Technol. 25 (5), 607–617. https://doi.org/10.2118/4007-pa.

Bermúdez, A., Shabani, M., 2022. Numerical simulation of gas composition tracking in a gas transportation network. Energy 247, 123459. https://doi.org/10.1016/j.energy.2022.123459.

Brill, J.P., Mukherjee, H.K., 1999. Multiphase Flow in Wells. Henry L. Doherty Memorial Fund of AIME. Society of Petroleum Engineers, Dallas.

Brustad, S., Løken, K.-P., Waalmann, J.G., 2005. Hydrate prevention using MEG instead of MeOH: impact of experience from major Norwegian developments on technology selection for injection and recovery of MEG. In: Offshore Technology Conference, OTC-17355-MS. https://doi.org/10.4043/17355-MS.

Chaczykowski, M., Zarodkiewicz, P., 2017. Simulation of natural gas quality distribution for pipeline systems. Energy 134, 681–698. https://doi.org/10.1016/j.energy.2017.06.020.

Chaczykowski, M., Sund, F., Zarodkiewicz, P., Hope, S.M., 2018. Gas composition tracking in transient pipeline flow. J. Nat. Gas Sci. Eng. 55, 321–330. https://doi.org/10.1016/j.jngse.2018.03.014.

Chen, H., Zhou, L., Li, G., Hei, M., Wang, K., Ye, Y., Gong, J., 2025. Numerical simulation and analysis of a temperature field in subsea caisson, 151 (3), 04025015. https://doi.org/10.1061/JLEED9.EYENG-5719.

Chen, H., Shi, B., et al., 2024. Phase equilibrium calculation of acid/alcohol hydrocarbon and water system based on stability analysis. CIESC J. 75 (3), 789–800. https://doi.org/10.11949/0438-1157.20231235 (in Chinese).

Costa do Nascimento, D., Sum, A.K., Barbosa Neto, A.M., da Costa, M.C., 2025. Protic ionic liquids as thermodynamic methane hydrates inhibitors. J. Mol. Liq. 424, 127082. https://doi.org/10.1016/j.molliq.2025.127082.

Epelle, E.I., Oyinbo, J.O., Okolie, J.A., Gerogiorgis, D.I., 2021. A comparative performance evaluation of cubic equations of state for predicting the compositional distribution of hydrate inhibitors in reservoir fluid systems. Fluid Phase Equilib. 535, 112964. https://doi.org/10.1016/j.fluid.2021.112964.

Epelle, E.I., Bennett, J., Abbas, H., Schmidt, K.A.G., Vesovic, V., 2020. Correlation of binary interaction coefficients for hydrate inhibition using the Soave-Redlich-Kwong equation of state and the Huron-Vidal mixing rule. J. Nat. Gas Sci. Eng. 77, 103259. https://doi.org/10.1016/j.jngse.2020.103259.

Fan, D., Gong, J., Zhang, S., Shi, G., Kang, Q., Xiao, Y., Wu, C., 2021. A transient composition tracking method for natural gas pipe networks. Energy 215, 119131. https://doi.org/10.1016/j.energy.2020.119131.

Folas, G.K., Berg, O.J., Solbraa, E., Fredheim, A.O., Kontogeorgis, G.M., Michelsen, M.L., Stenby, E.H., 2007. High-pressure vapor–liquid equilibria of systems containing ethylene glycol, water and methane: experimental

measurements and modeling. Fluid Phase Equilib. 251 (1), 52–58. https://doi.org/10.1016/j.fluid.2006.11.001.
Guandalini, G., Colbertaldo, P., Campanari, S., 2017. Dynamic modeling of natural gas quality within transport pipelines in presence of hydrogen injections. Appl. Energy 185, 1712–1723. https://doi.org/10.1016/j.apenergy.2016.03.006.
Huang, A., 2011. Inhibition of Gas Hydrate in Oil and Gas Transportation. Master's Thesis (in Chinese), China University of Petroleum (East China).
Huron, M.-J., Vidal, J., 1979. New mixing rules in simple equations of state for representing vapour-liquid equilibria of strongly non-ideal mixtures. Fluid Phase Equilib. 3 (4), 255–271. https://doi.org/10.1016/0378-3812(79)80001-1.
Javanmardi, J., Rasoolzadeh, A., Mohammadi, A.H., 2024. Development of a thermodynamic framework for modeling the heat of gas hydrate dissociation in the presence of poly n-vinyl caprolactam. Chem. Eng. Sci. 298, 120426. https://doi.org/10.1016/j.ces.2024.120426.
Jing, H., 2020. Multiphase Equilibrium Modeling for CO_2-hydrocarbon System. Master's Thesis (in Chinese). China University of Petroleum (Beijing). https://doi.org/10.27643/d.cnki.gsybu.2020.001658.
Kashish, Yusuf, M., et al., 2024. Natural gas hydrates: A review of various inhibitors and respective mechanisms. J. Mol. Liq. 403, 124809. https://doi.org/10.1016/j.molliq.2024.124809.
Katti, P.K., Chaudhri, M.M., 1964. Viscosities of binary mixtures of benzyl acetate with dioxane, aniline, and m-Cresol. J. Chem. Eng. Data 9 (3), 442–443. https://doi.org/10.1021/je60022a047.
Lei, W., Chen, D., Cheng, M., Cai, C., Wang, Q., 2025. Combined use of petroleum inclusion analysis, PVT simulation, and basin modeling for reconstruction of deep fluid phase evolution in condensate gas reservoirs. Mar. Petrol. Geol. 171, 107210. https://doi.org/10.1016/j.marpetgeo.2024.107210.
Li, W.-P., Lv, X.-F., et al., 2025. Multiphase flow characteristics of unconsolidated hydrate slurry in gas-water-hydrate-sand systems. Energy Fuel. 39 (9), 4260–4276. https://doi.org/10.1021/acs.energyfuels.4c06398.
Li, Y., Song, S., Liao, N., Chen, H., Yao, H., Shi, B., Gong, J., 2024. Molecular-level study on decomposition kinetics of CO_2–CH_4 hydrates. Energy Fuel. 38 (14), 12875–12887. https://doi.org/10.1021/acs.energyfuels.4c01796.
Li, Y., Song, S., et al., 2026. A transient model for oil-gas two-phase flow in undulating pipelines with multiple flow regimes. Int. Commun. Heat Mass Tran. 172, 110124. https://doi.org/10.1016/j.icheatmasstransfer.2025.110124.
Liu, L., Shi, B., et al., 2023. Co-deposition characteristics of hydrates and sands in gas-salty water-sands flow system. Fuel 346, 128276. https://doi.org/10.1016/j.fuel.2023.128276.
Lockhart, W., 1949. Proposed correlation of data for isothermal two-phase, two-component flow in pipes. Chem. Eng. Prog. 45 (1), 39–48.
Meng, Y., Han, B., et al., 2024. Hydrate blockage in subsea oil/gas pipelines: Characterization, detection, and engineering solutions. Engineering 46, 363–382. https://doi.org/10.1016/j.eng.2024.10.020.
Mukherjee, H., Brill, J.P., 1985. Pressure drop correlations for inclined two-phase flow. J. Energy Resour. Technol. 107 (4), 549–554. https://doi.org/10.1115/1.3231233.
Nasir, Q., Suleman, H., Elsheikh, Y.A., 2020. A review on the role and impact of various additives as promoters/inhibitors for gas hydrate formation. J. Nat. Gas Sci. Eng. 76, 103211. https://doi.org/10.1016/j.jngse.2020.103211.
Okuno, R., Johns, R.T.T., Sepehrnoori, K., 2010. A new algorithm for Rachford-Rice for multiphase compositional simulation. SPE J. 15 (2), 313–325. https://doi.org/10.2118/117752-PA.
Ovadia, S., 2006. Mechanistic Modeling of gas-liquid Two-phase Flow in Pipes. Society of Petroleum Engineers, Dallas. https://doi.org/10.2118/9781555631079.
Oyefunke Olarinoye, F., Kang, S.-P., Atubokiki Ajeinka, J., Sunday Ikiensikimama, S., 2024. Synergistic performance of mixed agro-waste-based amino acids as kinetic hydrate inhibitors for natural gas hydrate control. J. Mol. Liq. 395, 123837. https://doi.org/10.1016/j.molliq.2023.123837.
Peng, D.-Y., Robinson, D.B., 1976. A new two-constant equation of state. Ind. Eng. Chem. Fundam. 15 (1), 59–64. https://doi.org/10.1021/i160057a011.
Qi, J., Fan, D., Zhang, M., Song, S., Zhang, J., Shi, B., Gong, J., 2023. Component tracking and phase variation prediction of gas-liquid mixed transportation pipeline. Oil Gas Storage Transp. 42 (2), 215–222. https://doi.org/10.6047/j.issn.1000-8241.2023.02.011 (in Chinese).
Sahari Moghaddam, F., Mahmoodi, M., Zare, M., Goodarzi, F., Abdi, M., James, L., 2022. Natural gas hydrate equilibria in brine including the effect of inhibitors on hydrate formation. In: SPE Canadian Energy Technology Conference, SPE-208890-MS. https://doi.org/10.2118/208890-ms.
Song, S., Fan, D., et al., 2023. Research on transient composition tracking in natural gas condensate pipeline networks. Phys. Fluids 35 (2), 026102. https://doi.org/10.1063/5.0138237.
Sun, S., Gu, L., Yang, Z., Lin, H., Li, Y., 2022. Thermophysical properties of natural gas hydrates: A review. Nat. Gas. Ind. B 9 (3), 246–263. https://doi.org/10.1016/j.ngib.2022.04.003.
Taitel, Y., Dukler, A.E., 1976. A model for predicting flow regime transitions in horizontal and near horizontal gas-liquid flow. AIChE J. 22 (1), 47–55. https://doi.org/10.1002/aic.690220105.
Tianmin, G., 2002. Multi-element Gas-liquid Equilibrium and Distillation. Petroleum industry press, Beijing (in Chinese).
Wallis, G.B., 2020. One-dimensional Two-phase Flow. Courier Dover Publications, New York.
Wei, N., Pei, J., et al., 2024. Classification of natural gas hydrate resources: Review, application and prospect. Gas Sci. Eng. 124, 205269. https://doi.org/10.1016/j.jgsce.2024.205269.
Wei, Y., Worley, J., Zerpa, L.E., Chien, Y.-C., Dunn-Rankin, D., Kezirian, M.T., Koh, C.A., 2025. Natural gas storage in hydrates in the presence of thermodynamic hydrate promoters: Review and experimental investigation. Fluid Phase Equilib. 591, 114286. https://doi.org/10.1016/j.fluid.2024.114286.
Xin, Z., Jiang, Z., Wang, F., Zhang, Y., 2025. Review on flow assurance issues in natural gas pipeline transmission systems and solutions to hydrate deposition. Chem. Eng. Sci. 306, 121290. https://doi.org/10.1016/j.ces.2025.121290.
Yu, J., Song, S., et al., 2025. Prediction of hydrate formation temperatures in salt–alcohol inhibitor systems using an improved activity model. Energy Fuel. 39 (50), 23540–23555. https://doi.org/10.1021/acs.energyfuels.5c04711.
Yu, X., Feng, S., Li, Y., 2000. Derivation of temperature drop equations for multiphase flow pipes. Oil Gas Storage Transp. 19 (4), 22-25+58–25. https://doi.org/10.3969/j.issn.1000-8241-D.2000.04.008 (in Chinese).
Zhang, P., 2014. Modeling of pressure drop calculation by Beggs-Bril method for oil and gas mixing pipelines. Oil-Gas Field Surf. Eng. 33 (1), 35–36. https://doi.org/10.3969/j.issn.1006-6896.2014.1.021 (in Chinese).
Zhang, H., Wang, Q., Sarica, C., Brill, J.P., 2003. Unified model for gas-liquid pipe flow via slug dynamics—Part 1: Model development. J. Energy Resour. Technol. 125 (4), 266–273. https://doi.org/10.1115/1.1615246.